Acta Neuropathologica (2025) 150:6
https://doi.org/10.1007/s00401-025-02912-4

ORIGINAL PAPER

Amyloid-β plaque-associated microglia drive TSPO upregulation in Alzheimer's disease

Daniel A. Martinez-Perez[1] · Jennifer L. McGlothan[1] · Alexander N. Rodichkin[1] · Karam Abilmouna[1] · Zoran Bursac[2] · Francisco Lopera[3] · Carlos Andres Villegas-Lanau[3] · Tomás R. Guilarte[1]

Received: 3 April 2025 / Revised: 9 July 2025 / Accepted: 10 July 2025

Abstract

Translocator protein 18 kDA (TSPO) imaging using positron emission tomography (PET) is widely used to assess neuroinflammation in Alzheimer's disease (AD). However, the significance of the increase in brain TSPO levels in AD pathophysiology is not known. Here, we show that in the 5XFAD transgenic mouse model, brain TSPO levels increase in an age-, brain region-, and sex-dependent fashion. TSPO levels were first increased in the subiculum at 1.5 months of age in male and female 5XFAD mice compared to wildtype mice. The TSPO increase in the subiculum of 1.5-month 5XFAD mice coincided with the appearance of Aβ aggregation and increased serum $A\beta_{1\text{-}42}/A\beta_{1\text{-}40}$ ratio which occurred prior to increased serum neurofilament light chain (Nfl) levels and well before cognitive function deficits. We also discovered that the brain TSPO increase was driven by an expansion of activated microglia in contact with Aβ-plaques, that also expressed higher TSPO levels per microglia than microglia not in contact with plaques. While overall, astrocytes were highly activated, the increased TSPO signal in the 5XFAD mouse brain did not increase in astrocytes. We also compared the 5XFAD mouse findings to postmortem human brain tissue from early-onset autosomal-dominant Presenilin 1 (*PSEN1*)-*E280A* mutation AD cases. The results in *PSEN1-E280A* cases confirmed the 5XFAD mouse findings relevant to increased TSPO levels and an increase in TSPO per microglia contacting Aβ-plaques. In summary, TSPO is an early biomarker of neuroinflammation in the AD brain that first increases in the subiculum simultaneously with increased Aβ aggregation and serum $A\beta_{1\text{-}42}/A\beta_{1\text{-}40}$ ratio. The increased TSPO response in the 5XFAD mouse brain and in the brain from *PSEN1-E280A* mutation AD cases reflects Aβ-plaque-associated microglia with a high TSPO content. This microglia subtype is likely to promote the progression of AD pathology, neurodegeneration, and cognitive decline and their high TSPO content may serve as a target for TSPO ligand-based therapy.

Keywords Alzheimer's disease · Neuroinflammation · TSPO · Microglia · 5XFAD mice · *PSEN1-E280A* mutation

Introduction

Alzheimer's disease (AD) is a progressive neurodegenerative disorder in which neuroinflammation and glial cell activation play an important role in disease onset and progression [45–47]. Neuroinflammation is an early event that occurs with the early aggregation of amyloid-β (Aβ) fibrils that activate microglia to make contact with extracellular Aβ-plaques in an effort to phagocytize and remove them from the brain [20, 41]. This neuroinflammatory response occurs prior to the formation of intraneuronal hyperphosphorylated tau tangles, neurodegeneration, loss of brain volume, and cognitive decline, all of which are hallmark features of AD [18, 49, 69].

✉ Tomás R. Guilarte
tguilart@fiu.edu

[1] Brain, Behavior & the Environment Program, Department of Environmental Health Sciences, Robert Stempel College of Public Health & Social Work, Florida International University, Miami, FL 33199, USA

[2] Department of Biostatistics, Robert Stempel College of Public Health & Social Work, Florida International University, Miami, FL 33199, USA

[3] Neuroscience Group, Universidad de Antioquia, 050010 Medellín, Colombia

Published online: 17 July 2025

Translocator protein 18 kDa (TSPO) previously named the peripheral benzodiazepine receptor [58] is a glial stress-response protein that is expressed at low levels in the normal brain parenchyma [17, 31]. Experimental evidence indicates that in the normal brain, microglia and astrocytes express low levels of TSPO with blood vessels being a significant source [7, 32]. However, following disruption of brain homeostasis, microglia and/or astrocytes set in motion a neuroinflammatory cascade and significantly increase TSPO expression, a response that varies according to the disease type, disease stage, and brain region [17, 31, 32, 75].

Studies using TSPO-PET imaging indicate that TSPO levels are significantly increased in the AD brain [10, 12, 16, 34, 35, 59, 62, 73, 80, 82] and in animal models of AD [38, 48, 52, 63, 70, 74, 76]. A recent cross-sectional study in AD patients showed that neuroinflammation measured with TSPO-PET was associated with higher Aβ-plaques and tau burden [67]. Furthermore, TSPO levels were inversely associated with cognitive function deficits measured with the Mini-Mental State Examination and domain-specific tests [67]. These findings strongly suggest a putative role of TSPO in AD onset and progression. However, no previous human or animal study has determined how early in time and which brain region(s) first increase TSPO levels in the AD brain and what is the functional significance of the TSPO increase [4, 8, 25, 28, 33, 34, 52, 81]. Furthermore, a quantitative analysis and delineation of the cellular sources of the TSPO response and its association with AD pathology is important for appropriate interpretation of TSPO-PET imaging studies and understanding pathological mechanisms.

Previous studies determining the TSPO response in different preclinical animal models of AD [38, 48, 52, 63, 70, 74, 76] have used transgenic mice expressing human mutations in AD risk genes that are more representative of early-onset familial AD (EOAD) than late-onset sporadic AD (LOAD) cases. For example, preclinical models such as the 5XFAD mice express an aggressive behavioral and pathological temporal phenotype [26, 52, 54]. Relevant to this observation, studies in which the TSPO response in transgenic animal models have been compared to human AD cases, for the most part, have been compared to human brain tissue from LOAD cases [37, 53, 74, 75]. While these studies have provided valuable information, they can be confounded by the aggressive and rapid AD pathology and cognitive decline in transgenic mice when compared to the slow progression of human LOAD cases. Such differences in the rate of disease progression and brain age can potentially influence microglia function(s) and their TSPO response to AD pathology [24, 41]. Therefore, it is important to compare the TSPO response in transgenic animal models such as 5XFAD mice to brain tissue from human EOAD familial cases with a similar aggressive AD pathology and cognitive decline.

In the present study, we used a comprehensive approach from behavior to molecules in assessing the TSPO response in the 5XFAD mouse model using a life course approach. The 5XFAD mice is a widely used model expressing five human AD mutations [54] and we compared the TSPO results to postmortem human brain tissue from individuals carrying the Presenilin 1 (*PSEN1)-E280A* mutation (the Paisa mutation). These EOAD familial cases resemble the aggressive behavioral and pathological temporal phenotype as in the 5XFAD mouse model since patients display an aggressive temporal progression of AD pathology and cognitive decline beginning in the third decade of life with death occurring in the fifth decade of life [1, 2, 23]. In the 5XFAD mouse studies, we used a life course approach to closely examine how early in time and which brain region(s) TSPO levels increase in the early phase of the disease in relation to cognitive function changes, serum AD and neurodegeneration biomarkers as well as brain AD pathology. Furthermore, we examined the cellular sources of the TSPO response and its association with Aβ plaques to obtain information relevant to the interpretation of TSPO-PET studies.

Our results demonstrate that in the 5XFAD mouse model, TSPO levels exhibit an early increase at 1.5 months of age in the subiculum of male and female mice relative to wildtype (WT) mice followed by other AD-relevant brain regions where the TSPO increase did not start until 3, 7, or 12 months of age and it was sex dependent. The increase in brain TSPO levels in the subiculum of male and female 5XFAD mice occurred well before the appearance of cognitive function deficits and was due to an expansion in the number of activated microglia contacting Aβ plaques. We discovered that plaque-associated microglia expressed higher TSPO levels per microglia compared to microglia not contacting plaques and the TSPO increase in the 5XFAD mouse brain was not associated with astrocytes at any age. Finally, the TSPO findings in the 5XFAD murine model were confirmed in brain tissue from *PSEN1-E280A* mutation AD cases validating the 5XFAD mouse results.

Materials and methods

Animal husbandry and colony maintenance

The mouse strain used was B6SJL-Tg (APPSwFlLon, PSEN1*M146L*L286V) 6799Vas/Mmjax(5XFAD, RRID: MMRRC_034840-JAX; Mutant Mouse Resource and Research Center (MMRRC), The Jackson Laboratory, Bar Harbor, ME)., 5XFAD mice overexpress mutant human amyloid beta (A4) precursor protein 695 (APP) with the Swedish (K670N, M671L), Florida (I716V), and London (V717I) familial Alzheimer's disease mutations along with human presenilin 1 (PSEN1) harboring two familial AD

mutations, M146L and L286V [54]. The 5XFAD mouse colony was maintained by crossing 5XFAD hemizygous males with B6SJLF1/J females (stock #100012, The Jackson Laboratory, Bar Harbor, ME). The 5XFAD mice were compared with control WT mice, products of breeding within the colony. All mice were housed in specific pathogen-free (SPF) housing at 18–20 °C on a 12:12 light:dark cycle with ad-libitum food and water access. The aggressive phenotype of the 5XFAD mouse model results in death of some mice, especially in the 5XFAD female mice when aged to 12 months (Suppl. Table 1). All animal studies were reviewed and approved by the Florida International University Animal Care and Use Committee, comply with the ARRIVE guidelines, and were carried out following the National Institutes of Health Guide for the Care and Use of Laboratory Animals.

Mouse genotyping

A small tail snip was taken for genotyping at postnatal day 14 using a pair of sterilized scissors. DNA was extracted with Quickextract ^{tm} DNA extraction solution (Lucigen, QE09050, Middlesex, UK) following manufacturer instructions. PCR primer sequences used can be found in Suppl. Table 2. The PCR reaction occurred following protocols provided by The Jackson Laboratory. Electrophoresis was performed in a 1.5% agarose gel with gel red (3.75 µl/100 ml; Biotium, 41003, Fremont, CA) at 100 V for 60 min, and visualized using the Biorad Chemidoc XRS Imaging system (Bio-Rad Laboratories, Inc., Hercules, CA).

Experimental schedule

To explore a life-course approach for modeling AD, 5XFAD male and female mice with their respective WT controls were used at 1.5, 3, 7, and 12 months of age. At each time point, the animals were weighed, and neuropathological, molecular, and neurobehavioral assessments were performed. For any one measure, only 1 male and 1 female per genotype were used per litter, thus, the litter is the statistical unit.

Elevated plus maze (EPM)

EPM was implemented to assess anxiety-like behavior in mice [40, 79]. The EPM was elevated 50 cm off the floor and had 2 open arms and 2 closed arms with 40 cm high walls, each arm being 5 cm wide and 30 cm long. Briefly, each mouse was introduced in the center of the EPM and allowed to explore for 10 min. All trials were recorded and analyzed for time spent in each arm using EthoVision XT (Noldus, Leesburg, VA) in a blinded fashion.

Open field locomotor activity

Analysis of locomotor behavior was performed as described in Ref. [65]. The variables of interest were total distance traveled (cm), speed (cm/s), and resting time (s).

Barnes maze (BM)

The BM was implemented to evaluate spatial learning using a protocol adapted from those previously described [5, 61]. The maze has 20 evenly spaced holes, with an escape box (EB) located in a fixed location under one of the holes. Visual cues were maintained around the perimeter of the maze, and bright light and white noise were used as weak aversive stimuli. Prior to each trial, the mouse was placed in the center of the maze under an opaque box for 10 s after which it was allowed to move and latency (in seconds) to find the EB was recorded. Briefly, all mice experienced three test phases: the first was habituation (Day 1), in which the mouse was placed in the maze for a 60-s trial or until EB entry; the second phase was the acquisition (training) of the learning task (Days 2–6), when the animal was placed in the center of the maze for two trials (approximately 20 min apart) for 2 min or until EB entry; and the last phase was the probe test (Day 7), where the EB was removed and the animal was allowed to explore the maze for 60 s and the time spent in the quadrant containing the EB was recorded. At the end of each trial, the mice remained in the EB for 60 s before returning to their home cage. All trials were recorded and analyzed for latency to the EB, distance traveled, and speed using EthoVision XT (Noldus, Leesburg, VA).

Aβ immunohistochemistry

Free-floating brain sections from PFA-perfused WT and 5XFAD male and female mice at all assessed ages were sectioned at 40 µm and stored as previously described [65]. Brain sections at 1.94, 0.48, -1.94, and -3.40 from Bregma based on the Paxinos and Watson mouse brain atlas were selected. Immunohistochemistry was performed using standard protocols in our laboratory as previously described [65] with the following modifications. Tissue was incubated in primary antibody overnight at room temperature (RT), and a biotinylated secondary antibody for 1 h at RT. Information for all antibodies used can be found in Suppl. Table 3. Sections were developed in 3,3′-diaminobenzidine for 2 min at RT (DAB kit, SK-4100, Vector Laboratories, Burlingame, CA) and mounted on slides, dehydrated, and coverslipped. Images were captured using the BZ-X810 Microscope (Keyence Corporation, Itasca, IL).

Aβ-plaques load quantification

Image J version 1.50b (National Institute of Health) was used to quantify the Aβ-plaque load. First, DAB-stained MOAB-2 ($Aβ_{40-42}$) images at 2 × magnification from 5XFAD male and female mouse brains were converted to 8-bit. The scale size was set based on the image scale bar (2000 µm). For masking the background threshold was established based on the absence of unspecific staining by region and total coverage of the plaques. The images were processed to binary and watershed function to distinguish between each of the plaques, and each ROI was analyzed including the frontal cortex, the deep cortical layers, septal nuclei, hippocampus, thalamus, amygdala, and subiculum at each selected Bregma coordinate. The "analyze particles" function was used to calculate the number and the percent of the area covered by the Aβ-plaques.

TSPO quantitative autoradiography in the mouse brain

Fresh frozen brain tissue was obtained from animals at specific time points, cryosectioned at 20 µm in the coronal plane, and mounted onto poly-l-lysine coated microscopy slides. Two adjacent slides containing a representation of the coronal plane of the brain from each animal were selected for autoradiography incubations, one slide for total radioligand binding and the second slide for non-specific radioligand binding. Subsequent subtraction of non-specific ligand binding from the total ligand binding enables the determination of specific ligand binding to its target (TSPO). [^{3}H]-DPA-713 (final concentration ~ 1 nM) was used following an established protocol previously described [51]. Films were developed after 5 weeks of exposure, the resulting images were captured, converted into pseudo-color images, and quantified using internal standards (fmol/mg tissue) and MCID core 7.1 software (InterFocus Ltd. Linton, England). Multiple brain regions were analyzed including the frontal cortex, the deep cortical layers, septal nuclei, hippocampus, subiculum, thalamus, and amygdala at selected Bregma coordinate. The assays were performed at different times for males and females at each individual age.

Quadruple immunofluorescence staining in mouse brain tissue

Free-floating brains sections at Bregma − 1.94 and − 3.40 were used. The sections were washed in 1 × PBS, pH 7.4 at RT. Antigen retrieval was performed using 10 mM sodium citrate buffer at 37 °C for 30 min, followed by a 20-min incubation at RT. Then, they were blocked with 4% normal donkey serum (NDS) (Abcam, Cambridge, MA; ab7475) containing 0.5% Triton X-100 and 0.05% tween-20 for 1 h, followed by primary antibody incubation combinations for MOAB-2, TSPO, GFAP, Iba1, or CD31 at RT overnight. After washing, sections were incubated with 4% NDS and appropriate Alexa Fluor secondary antibodies for 1 h at RT, followed by washes. Information for all antibodies used can be found in Suppl. Table 3. Sections were mounted on slides and coverslipped with Prolong Gold Antifade mounting medium without DAPI (ThermoFisher Scientific, Waltham, MA; P36934) to preserve the signal intensity and brightness.

Determination of neurofilament light chain and $Aβ_{1-42}/Aβ_{1-40}$ ratio in serum

Serum was collected for neurofilament light chain (Nfl) and $Aβ_{1-42}/Aβ_{1-40}$ ratio from WT and 5XFAD male and female mice at all ages. Blood was collected from anesthetized animals by transcardial puncture and placed in a microtainer tube, kept 20 min at 4 °C to allow clot formation, centrifuged at 12,000 g for 15 min at 4 °C, and then frozen at -80 °C until used. All the samples were analyzed using the multiplate reader MESO Quick Plex SQ 120MM (MesoScale Diagnostics, Rockville, MD). To determine the Nfl levels in serum (pg/ml) R-PLEX Human Neurofilament L Assay (MesoScale Diagnostics, K1517XR, Rockville, MD) and to determine the $Aβ_{1-40}$ and $Aβ_{1-42}$ peptides serum concentration (pg/ml) V-PLEX Aβ Peptide Panel 1 (4G8) Kit Assay (MesoScale Diagnostics, K15199E, Rockville, MD) were utilized following manufacturer protocols. The $Aβ_{1-42}/Aβ_{1-40}$ ratio was calculated by dividing the concentration of $Aβ_{1-42}$ by $Aβ_{1-40}$.

Post-mortem brain samples from control and EOAD *PSEN1* (*E280A* mutation) patients

Nine brain samples were obtained from the Neuroscience Group at the Universidad de Antioquia (Colombia) brain bank. One control sample was eliminated from analysis due to excessive inflammation in the brain as a result of drug addiction. Patient information and characteristics are described in Suppl. Tables 4 and 5. Brain donations were obtained after informed consent and approval from the Institutional Review Board (IRB) of the Medical Research Institute, School of Medicine, Universidad de Antioquia. Written informed consent was obtained from donor's legal authorized proxies following the guidelines of the Code of Ethics of the World Medical Association, Helsinki declaration and Belmont Report.

Quantitative autoradiography for TSPO in postmortem human brains

We performed quantitative autoradiography using [^{3}H]-R-PK11195 (final concentration ~ 1 nM) on sections

from the medial Frontal Gyrus (Prefrontal Cortex) of human EOAD and control cases following the same protocol as in mice. In the mouse studies, we used the second-generation ligand [^{3}H]-DPA-713 because mice do not express the human *rs6971 TSPO* polymorphism that alters the TSPO affinity for second-generation ligands such as DPA-713 in human PET studies [56, 66]. Furthermore, [^{3}H]-DPA-713 has essentially no non-specific binding and provides a robust-specific binding signal. In the human studies, since we had a limited number of human brain samples, we used [^{3}H]-R-PK11195 because its binding to TSPO is not affected by the *rs6971 TSPO* polymorphism [57]. Eight slides containing two representative sections of the region from each brain were selected, four slides were used for total radioligand binding and the other four slides were used for non-specific radioligand binding. Films were developed after 8 weeks and analyzed blinded the same using MCID core 7.1 software (InterFocus Ltd, Linton, England). To distinguish the white and gray matter, the slides were stained with Nissl.

Quadruple immunofluorescence staining in postmortem human brain tissue

Paraffin-embedded brain slices of 5 µm from EOAD patients and controls on slides were heated in an oven at 60 °C for 2 h. Antigen retrieval was done using Antigen Unmasking Solution, Citrate-Based (Vector Laboratories, Burlingame, CA, H-3300-250) following manufacturer instructions. The slides were then permeabilized with a PBS 1x + triton X-100 (10%) solution for 5 min, then incubated with Sudan Black B (Millipore, Burlington, MA; 199664-25G) solution (1 gr/100 ml of ethanol 70%) for 10 min. Next, slides were blocked with 4% NDS (Abcam, Cambridge, MA; ab7475), 0.5% Triton X-100 and 0.05% tween-20 for 2 h at RT, followed by primary antibody incubation for BAM-10, TSPO, GFAP, and Iba1 at 4 °C overnight. After washing, sections were incubated with 4% NDS and appropriate Alexa Fluor secondary antibodies. Information about all antibodies used can be found in Suppl. Table 3. Sections were mounted on slides and coverslipped with Prolong Gold Antifade mounting medium without DAPI (ThermoFisher Scientific, Waltham, MA; P36934).

Confocal imaging acquisition

Z-stacks of 35 planes were acquired in the CA1, CA3, and CA4 (hilus) of the hippocampus and subiculum in WT and 5XFAD male and female mice at all ages ($n = 3$–5). Five random regions were selected in controls and 5 regions where Aβ plaques were observed in EOAD, then Z-stacks of 10 planes in the gray matter of superior gyrus of the temporal cortex were acquired (EOAD $n = 4$; controls $n = 4$). The images were obtained at 60 × magnification using a laser scanning confocal microscope (Fluoview FV10i, Olympus, Center Valley, PA), utilizing the FV10 image software. Laser sensitivity and intensity were set based on the non-primary antibody control slide. Utilizing the FV10 image software 3D images were assembled using the 35 or 10 planes.

TSPO colocalization analysis

For the assessment of % TSPO colocalization with Iba-1 and GFAP, respectively, 5 [CA1 (2), CA3 (1), and CA4 (2)] and 3 [subiculum] random images from WT and 5XFAD mice and 3–5 images at superior temporal cortex per control and EOAD patients were exported to Imaris Microscopy Image Analysis Software (Oxford Instruments, Abingdon, Oxfordshire, UK). For image processing, the background of each channel was subtracted using the software background subtraction feature. New channels were generated in the colocalization feature, and the threshold of each channel was determined based on the software's complete selection of the signal. Two new channels were created (1) TSPO and Iba-1 colocalized channel, and (2) TSPO and GFAP colocalized channel. The % of volume A in B was used for the assessment.

Quantification of the microglia number and microglia TSPO volume

Immunofluorescence images were exported to Imaris Microscopy Image Analysis Software. A render of the microglia and Aβ channels was created using the machine-learning feature of the software and subtracting the background and small-intensity signal. The microglia size was filtered at 10.5 µm in mouse brains and 7.5 µm in postmortem human brains based on the software measuring function of the cell body. Then, a mask rendering of the TSPO channel in microglia was created, defining the outline of the TSPO signal. The number of microglia per 60 × field of view equivalent to 2.4696×10^7 µm^3 in mouse brains and 7.056×10^5 µm^3 in postmortem human brains, the TSPO volume per microglia, and proximity to Aβ plaques (contacting plaque or not contacting plaque) were calculated.

Statistical analysis

All data analyses were performed in GraphPad Prism 9 and SAS/STATv15.2. The data were examined for normality using the Kolmogorov–Smirnov test and homoscedasticity using Levine's test. Descriptive statistics for continuous outcome variables consisted of means with their standard errors and were generated by independent variables of sex, genotype, brain region and age group. For univariate comparisons of outcome variable means between genotype, sex, and age levels, we applied a two-sample t-test or ANOVA with

post hoc multiple comparisons using Sidak adjustments for multiplicity In few instances where the normality assumption was violated non-parametric equivalent tests such as the Mann–Whitney U test and Kruskal–Wallis' test were used with Dunn's correction to compare outcome distributional equality between levels of independent variables. To test all experimental conditions, we applied multivariable fixed and/or mixed general linear regression models (equivalent to multi-factor ANOVA with between and/or within factors) to test the main effects of independent variables along with pre-planned 2- and 3-way interactions. In some instances where significant interactions were detected, we performed simplified subgroup analyses to explain the source of differential effects. Sidak correction was applied for all multiple comparison adjustments. Results were considered significant at an alpha level of 0.05 along with consideration of magnitude of difference between conditions and their variability estimates. Complete statistical analysis results are provided in Suppl. Tables 6–20.

Results

Age- and sex-dependent behavioral deficits and overall health in 5XFAD mice

We performed behavioral studies to characterize the onset and progression of deficits in cognitive function, anxiety, and locomotor behavior in male and female 5XFAD mice and age-matched WT controls at 1.5, 3, 7, and 12 months of age. The behavioral studies were performed to compare the temporal profile of the increase in brain TSPO levels relative to the emergence of cognitive function and behavioral deficits.

Barnes maze

Figure 1 shows that the acquisition of the learning behavior measured with the Barnes maze was significantly different in 5XFAD female mice relative to WT mice at 7 months of age and persisted at 12 months of age (Fig. 1; Suppl. Table 6a and 6b). On the other hand, the acquisition of the learning behavior for the male 5XFAD mice did not differ from WT until 12 months of age (Fig. 1; Suppl. Table 6a). For the probe test, WT female mice spent significantly more time in the quadrant that contained the escape box relative to 5XFAD female mice at both 7 and 12 months of age consistent with their deficits in acquisition of the learning task. On the other hand, in the 5XFAD male mice at 12 months of age the probe test did not differ from WT male mice ($p = 0.119$) despite significant differences in the acquisition of the learning behavior (Fig. 1 Suppl. Table 6a and 6c). One potential explanation for the lack of differences in the probe test between WT and 5XFAD male mice at 12 months of age is that the WT male mice at 12 months of age, on average, spent less time in the quadrant with the escape box than at younger ages (Fig. 1). An effect that was not observed in WT female mice (Fig. 1; Suppl. Table 6a and 6c). Notably, spatial learning using the Barnes maze was not performed at 1.5 months of age because 5XFAD male or female mice did not exhibit learning deficits at 3 months of age. Collectively, the Barnes Maze results indicate significant deficits in cognitive performance in 5XFAD female mice relative to WT at 7 and 12 months of age, consistent with other studies using the same transgenic mouse model of AD [26]. On the other hand, learning deficits in male 5XFAD mice relative to WT were not observed until 12 months of age (Fig. 1; Suppl. Table 6a).

Elevated plus maze

We used the elevated plus maze to assess anxiety. Overall, there was an age- and genotype-dependent increase in the amount of time that the 5XFAD male and female mice spent in the open arms with a concomitant decrease in the time spent in the closed arms (Suppl. Figure 1a; Suppl. Tables 7a and 7b). The main differences in 5XFAD male and female mice spending more time in the open arms and less time in the closed arms relative to WT mice were at 12 months of age (Suppl Fig. 1a; Suppl. Tables 7a and 7b). These findings indicate that 5XFAD mice lose their normal innate fear behavior to seek refuge in the close arms of the elevated plus maze as AD pathology progresses in relevant brain structures such as hippocampus and amygdala and (Fig. 2 and Suppl. Figure 2).

Locomotor behavior

We used automated activity cages during the dark cycle to assess locomotor behavior. The results indicate a significant increase in total distance traveled in female 5XFAD mice relative to WT female mice (Genotype effect: $F_{1,65} = 24.4$; $p < 0.0001$; Suppl Fig. 1b; Suppl. Table 7a). No effect was observed between male WT and 5XFAD mice at any age (Suppl Fig. 1b; Suppl. Table 7a), confirming a sex effect driven by the 5XFAD female mice (Sex effect: $F_{1,131} = 21.4$; $p < 0.0001$ see Suppl. Table 20). For average speed and resting time, we found a significant sex effect (Sex effect of average speed $F_{1,131} = 13.1$; $p < 0.0004$; sex effect for resting time: $F_{1,131} = 9.97$; $p = 0.002$ see Suppl. Table 20). Furthermore, we also found a significant genotype effect ($F_{1,131} = 4.97$; $p = 0.03$) for resting time with the 5XFAD mice having an overall decrease in resting time (Suppl Fig. 1b; Suppl. Table 7a).

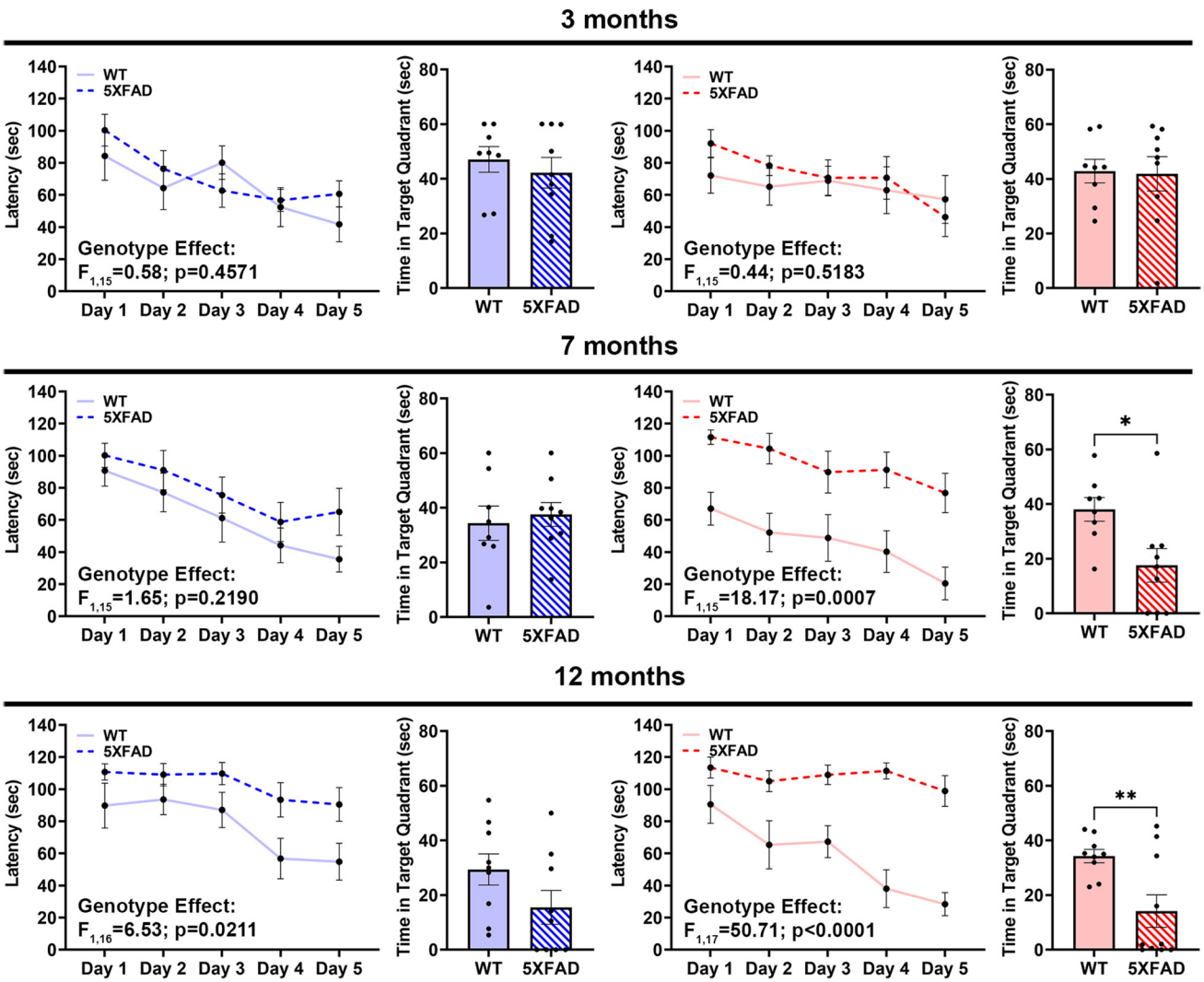

Fig. 1 Barnes maze spatial learning assessment of WT and 5XFAD mice. Learning curves in the acquisition of the Barnes maze task by male (blue panels) and female (red panels) WT ($n=8$–9) and 5XFAD ($n=9$–10) mice. Each data point represents the time (latency) in seconds to enter the escape box and is the average of 2 trials per day. Acquisition curve data were analyzed using a two-way ANOVA (genotype and trial days) with repeated measures (trial days) with Šídák's multiple comparisons test for comparisons at each age. Bar graphs represent Probe test performance 24 h after the last training day and were analyzed by a two-sample t-test at each age. All data are represented as mean ± SEM. $^{*}p<0.05$, $^{**}p<0.01$. Complete statistical analysis for Barnes Maze results is presented in Suppl. Table 6A-C and 20

Body weight

We also measure body weight of all mice as a function of age (Suppl. Fig. 1c). The result indicates that male and female 5XFAD mice lose significant body weight as a function of age relative to WT mice (Genotype effect: $F_{1,139}=80.5$; $p<0.0001$; Suppl. Tables 7a and 7b). Female 5XFAD mice had a greater decrease in body weight than male 5XFAD mice at 7 months relative to WT (male % decrease: 16%; female % decrease; 22%) and at 12 months of age (male % decrease: 34%; female % decrease; 44%) (Suppl. Figure 1c; Suppl. Tables 7a and 7b). Finally, approximately 14.7% of the 5XFAD mice die by 12 months of age, consistent with the aggressive EOAD phenotype. This effect was primarily driven by 5XFAD female mice accounting for 9.2% of the total deaths (Suppl. Table 1). Collectively, these findings indicated an aggressive progression of behavioral deficits and health deterioration in 5XFAD mice consistent with an EOAD etiology.

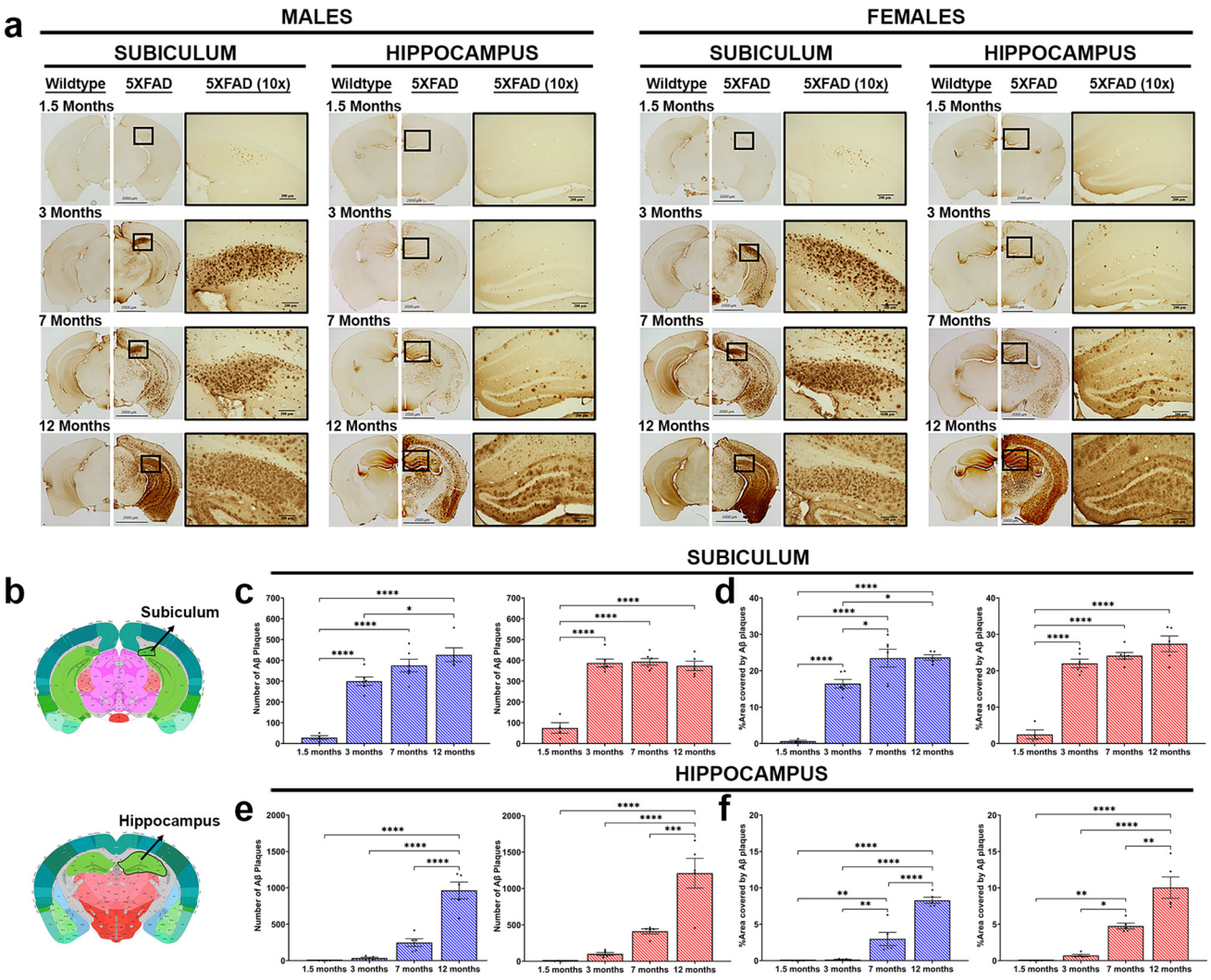

Fig. 2 Analysis of Aβ plaque load in the subiculum and hippocampus of 5XFAD mice as a function of age. **a** Representative images of Aβ staining with MOAB-2 ($Aβ_{40-42}$) by diaminobenzidine immunohistochemistry showing overall plaque load at the level of bregma − 3.40 (subiculum), and bregma − 1.94 (hippocampus) in male (blue panels) and female (red panels) WT ($n = 4–5$) and 5XFAD ($n = 4–6$) mice at 2X and 10X magnification. **b** Outlines of analyzed ROI: subiculum (top) and bottom (hippocampus), taken from the Atlas brain map (https://atlas.brain-map.org/). **c** Number of Aβ plaques and **d** % area covered by the Aβ plaques in the subiculum. **e** Number of Aβ plaques and **f** % area covered by the Aβ plaques in the hippocampus CA4 region. Data were analyzed by one-way ANOVA (age) with Šídák's multiple comparisons test for comparisons by age. All data are represented as mean ± SEM. $*p < 0.05$, $**p < 0.01$, $***p < 0.001$, $****p < 0.0001$. Complete statistical analysis for Aβ plaque load results is presented in Suppl. Table 8a, b and 20

Quantitative analysis of brain Aβ-plaques, serum $Aβ_{1-42}/Aβ_{1-40}$ ratio and neurofilament light chain (Nfl) concentrations in 5XFAD and WT mice

Aβ-plaques

To assess the progression of AD pathology in the 5XFAD mice, we measured the number of Aβ-plaques and percent brain area covered by Aβ-plaques in several brain regions including the subiculum, hippocampus, cerebral cortex (deep cortical layers), septal nucleus, amygdala, and thalamus of 5XFAD male and female mice from 1.5 to 12 months of age. Figure 2 and Suppl. Figure 2 show that Aβ-plaque number and percent area covered by plaques increased as a function of age in 5XFAD male and female mice in all brain regions. The subiculum was the brain region in which Aβ aggregation first appeared in the 5XFAD mouse brain at 1.5 months of age (Fig. 2a and 2c; Suppl. Tables 8a and 8b) consistent with the subiculum being a brain region with early atrophy in human AD cases [13, 71]. Furthermore, there were age x sex interaction ($F_{3,34} = 3.31$; $p = 0.035$; Suppl. Table 20) in the number of Aβ-plaques in the subiculum with female 5XFAD mice having a greater number of plaques at an earlier age than in 5XFAD males. Aβ-plaques in other brain

regions such as the hippocampus, frontal cortex, deep layers of the cerebral cortex, thalamus, septal nucleus, and amygdala were increased at 3 or 7 months of age and progressed with aging (Suppl. Figure 2; Suppl. Tables 9a and 9b). Overall, there was a higher Aβ-plaque load in 5XFAD female in the deep layers of the cerebral cortex and amygdala than in 5XFAD males (Suppl. Figure 2 and Suppl. Table 20).

Serum AD markers

Serum $A\beta_{1\text{-}42}/A\beta_{1\text{-}40}$ ratio and Nfl levels representative of AD pathology and ongoing neurodegeneration [15, 68], respectively, were measured as a function of age and sex in 5XFAD and WT mice using a MSD multiplex assay. Figure 3a shows that the serum $A\beta_{1\text{-}42}/A\beta_{1\text{-}40}$ ratio was significantly increased at 1.5 months of age in 5XFAD mice relative to WT and the ratio decreased in both male and female 5XFAD mice with age (Suppl. Tables 10a and 10b). Overall, there were higher levels of $A\beta_{1\text{-}42}/A\beta_{1\text{-}40}$ ratio in female 5XFAD mice compared to 5XFAD male mice (sex effect: $F_{1,64}=7.92$; $p=0.0065$; see Suppl. Table 20). Serum concentrations of $A\beta_{1\text{-}42}$ and $A\beta_{1\text{-}40}$ peptides by sex and age are provided in Suppl. Figure 3; Suppl. Tables 11a and 11b.

Analysis of serum Nfl concentrations in male and female 5XFAD mice significantly increased at 7 and 12 months of age compared to WT (Fig. 3b; Suppl. Tables 10a and 10b). Collectively, these results indicate that the subiculum is the brain region that first expresses Aβ-plaques, consistent with elevated serum $A\beta_{1\text{-}42}/A\beta_{1\text{-}40}$ ratio measured at the same age. Serum $A\beta_{1\text{-}42}/A\beta_{1\text{-}40}$ ratio decreased with age as plaque load increased in the brain. The latter indicates that as brain plaque load increases, serum $A\beta_{1\text{-}42}/A\beta_{1\text{-}40}$ ratio decreases as more of the Aβ peptides are retained in the brain. Importantly, from a temporal perspective, increased serum $A\beta_{1\text{-}42}/A\beta_{1\text{-}40}$ ratio preceded the increase in serum Nfl levels (Fig. 3).

TSPO levels in the 5XFAD mouse brain increase in an age-, sex-, and brain-region dependent fashion

Quantitative autoradiography with the TSPO-specific radioligand [^{3}H]-DPA-713 was used to determine TSPO levels in several brain regions as a function of age and sex in 5XFAD and WT mice. Figure 4 shows that TSPO levels first increased in the subiculum of male and female 5XFAD mice at 1.5 months of age relative to WT and TSPO levels

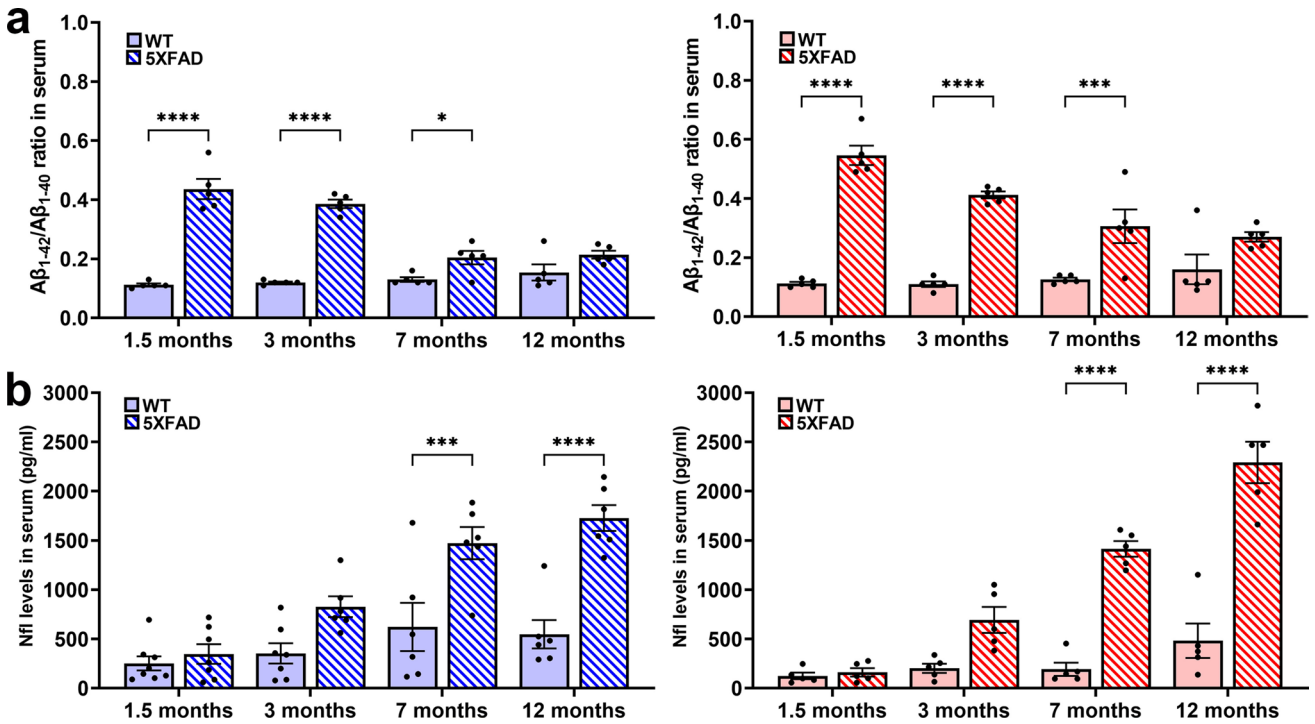

Fig. 3 Analysis of $A\beta_{1\text{-}42}/A\beta_{1\text{-}40}$ ratio and neurofilament light chain levels in serum of WT and 5XFAD mice as a function of age. **a** $A\beta_{1\text{-}42}/A\beta_{1\text{-}40}$ ratio in serum of male (blue panels) and female (red panels) WT ($n=5$) and 5XFAD ($n=5$) mice. **b** Neurofilament light chain (Nfl) levels (pg/ml) in serum of male (blue panels) and female (red panels) WT ($n=5$–8) and 5XFAD ($n=5$–7) mice. Data were analyzed by two-way ANOVA (genotype and age) with Šídák's multiple comparisons test for comparisons by age-matched genotype. All data are represented as mean ± SEM. $^*p<0.05$, $^{***}p<0.001$, $^{****}p<0.0001$. Complete statistical analysis for $A\beta_{1\text{-}42}/A\beta_{1\text{-}40}$ ratio in serum results is presented in Suppl. Tables 10a, b and 20

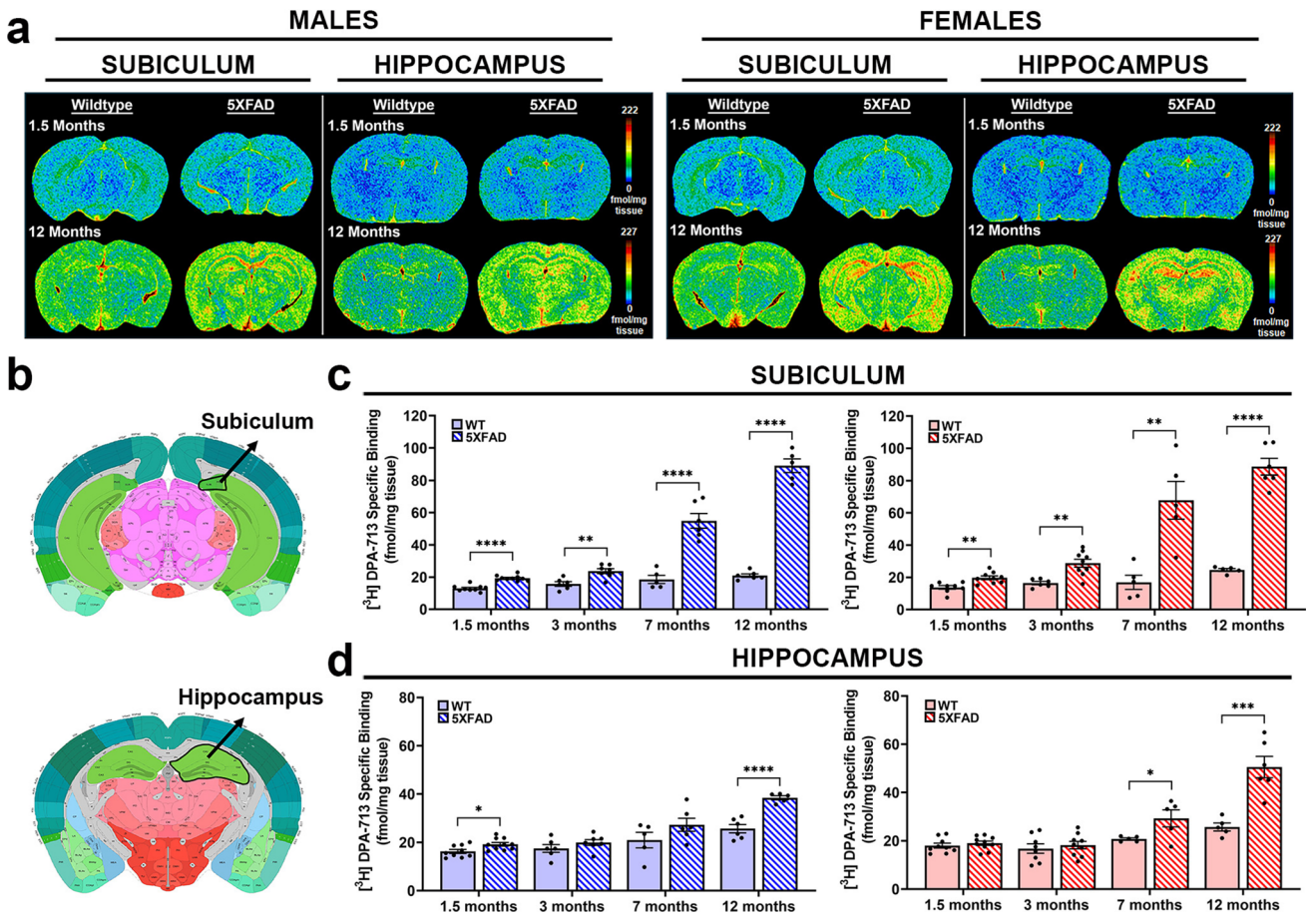

Fig. 4 Brain TSPO levels in the subiculum and hippocampus of WT and 5XFAD mice using by [^{3}H]-DPA-713 quantitative autoradiography as a function of age. **a** Representative pseudocolor images with calibration bars of [^{3}H]-DPA-713 autoradiography at the level of bregma − 3.40 (subiculum), and bregma − 1.94 (hippocampus) of male (left) and female (right) WT and 5XFAD mice at 1.5 and 12 months of age. **b** Outlines of Analyzed ROI: subiculum (top) and hippocampus (bottom), taken from the Atlas brain map (https://atlas.brain-map.org/). TSPO-specific binding levels (fmol/mg tissue) in the **c** subiculum and **d** hippocampus of male (blue panels) and female (red panels) WT (n = 4–10) and 5XFAD (n = 4–9) mice. Data were analyzed by two-way ANOVA (genotype and age) with Šídák's multiple comparisons test for comparisons with subgroup analysis at each age-by-age-matched genotype. All data are represented as mean ± SEM. *$p < 0.05$, **$p < 0.01$, ***$p < 0.001$, ****$p < 0.0001$. Complete statistical analysis for TSPO autoradiography results is presented in Suppl. Tables 12a, b and 20

continued to increase in the subiculum of 5XFAD mice as a function of age (Fig. 4 and Suppl. Tables 12a and 12b). Analysis of other AD-relevant brain regions shows that TSPO levels were also increased in the hippocampus of 5XFAD male mice at 1.5 months of age, but not in female mice (Fig. 4; Suppl. Tables 12a and 12b). TSPO levels in the frontal cortex, septal nuclei, and thalamus of 5XFAD male mice were not significantly increased until 3 months of age relative to WT mice (Suppl. Figure 4; Suppl. Tables 13a and 13b). A similar age-dependent TSPO increase occurred in these brain regions at 3 months of age in female 5XFAD mice except in the thalamus when TSPO levels significantly increased at 7 months of age (Suppl. Figure 4; Suppl. Tables 13a and 13b). Finally, TSPO levels in the deep cortical layers and amygdala of 5XFAD female mice were significantly different from WT at 7 and 12 months, while in male 5XFAD mice, the increase occurred at 12 months of age (Suppl. Figure 4; Suppl. Tables 13a and 13b). We also found a significant sex difference with females expressing higher TSPO levels in the deep cortical layers at Bregma 0.48 ($F_{1,95} = 5.38$; $p = 0.02$) and in the thalamus ($F_{1,94} = 5.95$; $p = 0.016$) (Suppl. Table 20). These findings indicate that the subiculum is the first brain region in which TSPO levels increase in 5XFAD male and female mice and the TSPO increase occurs well before cognitive function deficits at 12 months of age in males and 7 months of age in females. In summary, TSPO is an early biomarker of neuroinflammation starting in the subiculum and progressing to other brain regions. Finally, analysis of TSPO levels in different brain regions of WT male and female mice showed a significant

and progressive increase with aging (Fig. 4c and 4i; Suppl Fig. 4c-h; Suppl. Tables 14a, 14b, 13a and 13b).

Cellular sources of the TSPO response in the 5XFAD mouse brain

An important aspect of human TSPO-PET imaging studies to assess neuroinflammation in AD and in other neurodegenerative and neurological disorders is to understand the cellular sources of the TSPO response to provide the correct interpretation of the PET study. While TSPO levels in AD have been shown to be associated with microglia and astrocytes [70, 74], no previous study has performed quantification of the colocalization of TSPO using quadruple-label immunofluorescence confocal imaging of TSPO, Aβ-plaques, microglia, and astrocytes at the same time in the same brain slice. This approach provides a comprehensive picture of the cellular sources of the TSPO response in the context of AD pathology derived from the same image since most of the TSPO signal is accounted for in either microglia or astrocytes. Furthermore, in the brain parenchyma a TSPO signal that is not associated with microglia or astrocytes is likely to be associated with blood vessels [7, 32].

Our results indicate that in the WT mouse brain, TSPO is present at low levels in the normal mouse brain parenchyma (Suppl. Figure 5). Furthermore, in WT mice, the majority of the TSPO signal was associated with blood vessels, with lower TSPO levels in astrocytes that are in physical contact with blood vessels, or with normal ramified microglia (Suppl. Figure 5). Figure 5 shows the results of quadruple label immunofluorescence confocal imaging z-stacks for Aβ-plaques (MOAB2), microglia (Iba-1), astrocytes (GFAP), and TSPO in the subiculum and CA4 region of the hippocampus. Figure 5a depicts images of individual signals, two signals combined, and all signals merged for 5XFAD male and female mice at 1.5 and 12 months of age. We selected an early and late age to demonstrate the dramatic increase in the TSPO signal. Figure 5c shows a high degree of TSPO colocalization with Iba-1 in microglia as shown by the close overlap of the signal intensities profiles for TSPO and Iba-1. In these brain regions, the degree of colocalization of TSPO with microglia increased as a function of age, and we found females had a higher amount of colocalization in the hippocampus when compared to males (sex effect $F_{1,43} = 7.71$; $p = 0.008$) (Fig. 5d and 5e; Suppl. Tables 14a and 14b; Suppl. Table 20). On the other hand, TSPO colocalization with astrocytes (GFAP) in 5XFAD and WT male and female mice did not change with age in any brain region (Suppl. Figure 6; Suppl. Tables 15a and 15b).

We analyzed the quadruple label immunofluorescence confocal images in the subiculum and hippocampus with Imaris image analysis software and were able to determine the number of microglia and categorize them into two groups: (1) microglia in physical contact within Aβ-plaques, or (2) microglia not in contact with Aβ-plaques irrespective of their distance from the Aβ-plaque in the image. In addition, once the microglia were categorized, we were able to measure the level of TSPO per each of these types of microglia. Figure 6a shows the progression of the analysis using the Imaris image analysis software. Figure 6a left panel depicts the triple label confocal immunofluorescence z-stack image of Aβ-plaques (MOAB-2), microglia (Iba-1), and TSPO. In this image, the astrocyte GFAP signal was eliminated to make it easier to demonstrate the TSPO colocalization with microglia. The middle panel in Fig. 6a is the rendering of the image using Imaris from which the analysis was performed. The image in the right panel is a magnification of the white square in the middle panel in which one can clearly see the high levels of TSPO in microglia contacting Aβ-plaques versus microglia that are not contacting plaques. Based on the image analysis with Imaris, we found that in the 5XFAD mouse brain there was an age-dependent increase in the number of microglia in the subiculum and hippocampus of 5XFAD male and female mice (Fig. 6b and 6f; Suppl. Tables 16a and 16b). With the expansion in the number of microglia at an early age in the subiculum than in the hippocampus (Fig. 6b and 6f). We also discovered that the number of microglia not contacting plaques did not appreciably change in the subiculum or hippocampus of male or female 5XFAD mice as a function of age (Fig. 6c and 6g; Suppl. Tables 16a and 16b), except for microglia not contacting plaques in the hippocampus of female 5XFAD mice at 12 months of age which decreased in number relative to 7 months of age (Fig. 6g). On the other hand, the number of microglia contacting Aβ-plaques significantly increased as a function of age in both brain regions from male and female 5XFAD mice with a higher number in the subiculum of female mice (sex effect $F_{1,21} = 8.46$; $p = 0.0084$) (Fig. 6d and 6h; Suppl. Tables 16a and 16b; Suppl. Table 20). We also measured the TSPO content of microglia that were in contact or not in contact with Aβ-plaques. The results in Fig. 6e and 6i indicate that the majority of the TSPO increase in the subiculum and hippocampus of 5XFAD male and female mice as a function of age (Suppl. Figure 7; Suppl. Tables 17) was driven by activated microglia that were in contact with Aβ-plaques.

Studies in postmortem brain tissue from early-onset autosomal-dominant *PSEN1-E280A* mutation AD cases confirms the 5XFAD mouse findings

We used cerebral cortex tissue from EOAD cases expressing the *PSEN1-E280A* mutation and healthy controls obtained from the Universidad de Antioquia Brain Bank (Medellin, Colombia). Tissue from the brain of these unique EOAD cases is highly desirable and has been widely used in

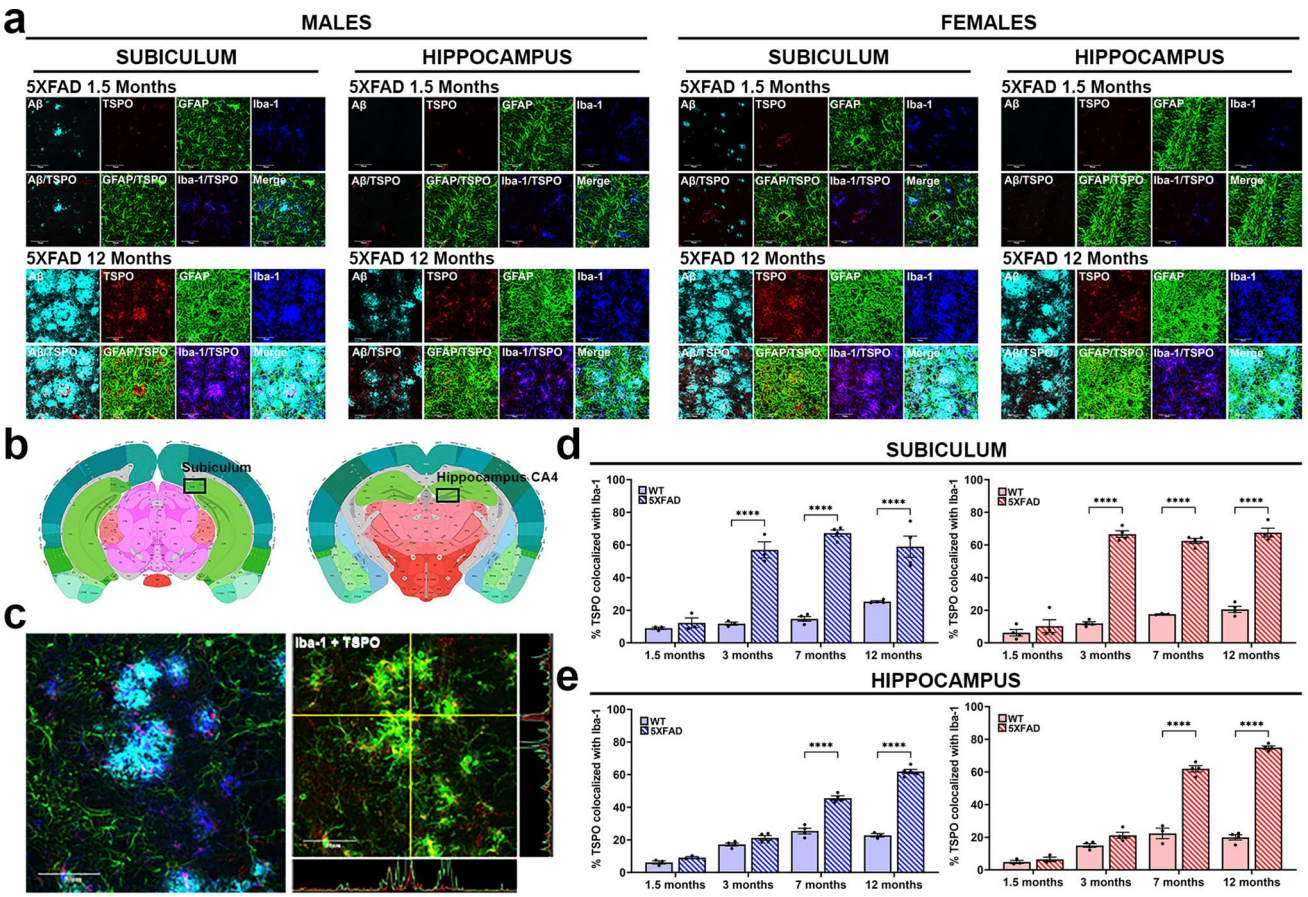

Fig. 5 Analysis of TSPO colocalization with microglia in WT and 5XFAD mice as a function of age. **a** Representative quadruple-label immunofluorescence confocal imaging z-stacks of Aβ (cyan), TSPO (red), astrocytes (GFAP; green), and microglia (Iba-1; blue) in the subiculum and CA4 region of the hippocampus of 1.5- and 12-month-old male (left panels) and female (right panels) WT and mice at 60X magnification. **b** Outlines of analyzed ROI: subiculum (left) and hippocampus-CA4 (right) taken from the Atlas brain map (https://atlas.brain-map.org/). **c** Intensity profile analysis using a representative confocal z-stack (left panel) from a 7-month 5XFAD female at the hippocampus-CA4 stained for Aβ (cyan), TSPO (red), astrocytes (GFAP; green), and microglia (Iba-1; blue). Intensity profiles were generated (right image) showing only TSPO (red) and microglia (Iba-1; green) with horizontal and vertical intensity lines showing overlapping peaks. Percent TSPO colocalization with Iba-1 using Imaris in the **d** subiculum and **e** hippocampus of male (blue panels) and female (red panels) WT ($n = 3$–5) and 5XFAD ($n = 3$–5). Data were analyzed by two-way ANOVA (genotype and age) with Šídák's multiple comparisons test for comparisons by age-matched genotype. All data are represented as mean ± SEM. ****$p < 0.0001$. Complete statistical analysis for TSPO colocalization results is presented in Suppl. Tables 14a, b and 20

previous studies; thus, we were not able to secure tissue from the hippocampus. Therefore, temporal and frontal cortex tissue were used for our studies. The average age at death of the EOAD cases was 58.3 ± 4.4 years of age and controls 61.8 ± 12.8 years of age (Suppl. Table 4). There was a significant difference in the brain weight (Suppl. Table 4; Suppl. Table 19) in the EOAD cases vs healthy control subjects and all subjects were male. The neuropathological classification of the EOAD cases was as follows: Braak stage 6, CERAD C, Thal 5, and NIA-AA A3, B3, C3 (Suppl. Table 5).

We performed TSPO quantitative autoradiography using the prototypical TSPO specific ligand [^{3}H]-R-PK11195 in frontal cortex tissue from *PSEN1-E280A* mutation AD cases and controls. Figure 7a depicts autoradiography images of total and non-specific binding in frontal cortex tissue from a control and *PSEN1-E280A* case. The graph in Fig. 7a shows that there is a significant increase in [^{3}H]-R-PK11195 specific binding to TSPO in gray and white matter in the frontal cortex of *PSEN1-E280A* cases relative to controls (Suppl. Table 18a). To determine the cellular sources of the TSPO response and the spatial relationship of TSPO-expressing glial cells with Aβ-plaques, we performed quadruple label immunofluorescence confocal imaging of TSPO, Aβ-plaques, microglia, and astrocytes in postmortem fixed and paraffin embedded temporal cortex tissue from *PSEN1-E280A* cases and controls as performed with the 5XFAD mouse studies. Figure 7b shows control and *PSEN1-E280A* quadruple label immunofluorescence confocal imaging

z-stacks demonstrating the high levels of astrocytes and microglia surrounding an Aβ-plaque.

We also performed image analysis of the immunofluorescence confocal images using Imaris imaging analysis software to determine microglia number, the classification of microglia based on their contact with Aβ-plaques and the level of TSPO per microglia as with the 5XFAD mouse results. One important advantage of the Imaris image analysis software is that it can separate individual microglia from a cluster of microglia using machine learning algorithms: thus, allowing individual microglia count as shown in Suppl Fig. 8. Figure 7c shows the immunofluorescence confocal image of Aβ-plaque, microglia and TSPO in the left panel, the rendering of the image using Imaris in the middle panel and the magnification of the rendering in the white square of the middle panel shown in the right panel. We discovered that similar to the results in the 5XFAD mouse brain, the increase in TSPO levels in *PSEN1-E280A* cases was also due to a significant increase in the number of microglia (Fig. 7d; Suppl. Table 18a) with microglia contacting Aβ-plaques expressing a higher TSPO level per microglia compared to microglia not contacting plaques (Fig. 7f; Suppl. Table 18b), despite a higher number of microglia not in contact with plaques (Fig. 7e; Suppl. Table 18a). Furthermore, like the 5XFAD results, TSPO colocalization is increased with microglia but did not change with astrocytes in the AD cases relative to controls (Suppl. Figure 9a and 9b; Suppl. Table 19). These findings show that when using the appropriate comparison of EOAD transgenic mice to brain tissue from human EOAD cases, the findings in the transgenic mouse model are consistent with those found in human EOAD subjects.

Discussion

To our knowledge, this is the first report that describes the relationship between brain TSPO levels, serum $A\beta_{1\text{-}42}/A\beta_{1\text{-}40}$ ratio and serum Nfl levels as well as Aβ-plaque number and brain area covered by plaques relative to cognitive function and behavioral deficits in 5XFAD male and female mice using a life course approach from an early stage of the disease (1.5 months) to a late stage (12 months). We found that TSPO was an early biomarker of neuroinflammation and disease progression since TSPO levels significantly increased in the subiculum of male and female 5XFAD mice at the early age of 1.5 months relative to WT. The TSPO increase in the subiculum of male and female 5XFAD mice at 1.5 months of age occurred well before deficits in cognitive function which were expressed at 7 months of age in female mice and at 12 months of age in male mice (Fig. 1). We also found that TSPO levels were closely associated with the early appearance of Aβ aggregates in the subiculum and increased serum $A\beta_{1\text{-}42}/A\beta_{1\text{-}40}$ ratio in male and female 5XFAD mice at 1.5 months of age (Fig. 2 and 3). Moreover, serum $A\beta_{1\text{-}42}/A\beta_{1\text{-}40}$ ratio decreased with age concurrently with the increase in brain Aβ-plaque number (Fig. 2 and 3) similar to what has been shown in human AD subjects and preclinical AD animal models [9, 21, 29]. We also discovered that the age-dependent TSPO increase in the 5XFAD mouse brain was primarily driven by an overall expansion in the number of microglia and an increase in TSPO level per microglia, specifically in microglia that were in contact with Aβ-plaques (Fig. 6).

Analysis of TSPO levels in WT male and female mice showed that TSPO levels increased in the WT mouse brain with aging (Fig. 4c and 4d; Suppl Fig. 4c–h; Suppl. Table 12a and 13a). This finding is consistent with previous studies in mice and human subjects demonstrating that TSPO levels increase with age in the normal brain. For example, Liu et al. used [^{18}F]-GE180 ex vivo PET imaging and autoradiography and found that TSPO levels increased in the hippocampus and cortex of mice aged to 26 months old when compared to 4 months old mice [48]. Moreover, TSPO was shown to increase in multiple brain regions, including pituitary gland, midbrain, thalamus, basal ganglia, occipital cortex, hippocampus and cerebellum in PK11195 PET scans of healthy adults when compared to those of healthy children [44]. In addition, [^{11}C]-PBR28 PET scans in healthy subjects ranging between 19 and 80 years of age revealed an increase in TSPO levels in the frontal and temporal cortex [78]. These findings indicate that brain TSPO levels increase with normal aging and should be considered in the interpretation of TSPO-PET imaging studies.

Previous studies have shown that in AD, microglia are associated with Aβ-plaques, and that these microglia expressed TSPO [14, 52, 63, 74]. However, our current work is the first report that quantitatively demonstrates that the TSPO increase in the AD brain was driven primarily by increased TSPO expression in microglia associated with Aβ-plaques (Fig. 6e and 6i). Importantly, the TSPO increase was not associated with astrocytes in any of the brain regions analyzed or at any age in 5XFAD mice despite significant astrocyte activation (Suppl. Figure 6). These findings are in contrasts with a study by Tournier et al., in which they described an increase in astrocytic TSPO prior to microglial TSPO in a transgenic rat model of AD [74]. It is possible that these differences may be due to the AD model used; that is mouse vs rat. Another possibility is that in the transgenic rat study by Tournier et al., [74], they injected a radioactive TSPO tracer into the animal, harvested the brain and dissociated it to identify cells that bind the TSPO radioligand. For this purpose, cell origin identification of TSPO binding was performed by sorting of astrocytes using glutamate transporter 1 (GLT1), Iba-1 for microglia, and CD31 for endothelial cells. However, GLT1 is not exclusively expressed in

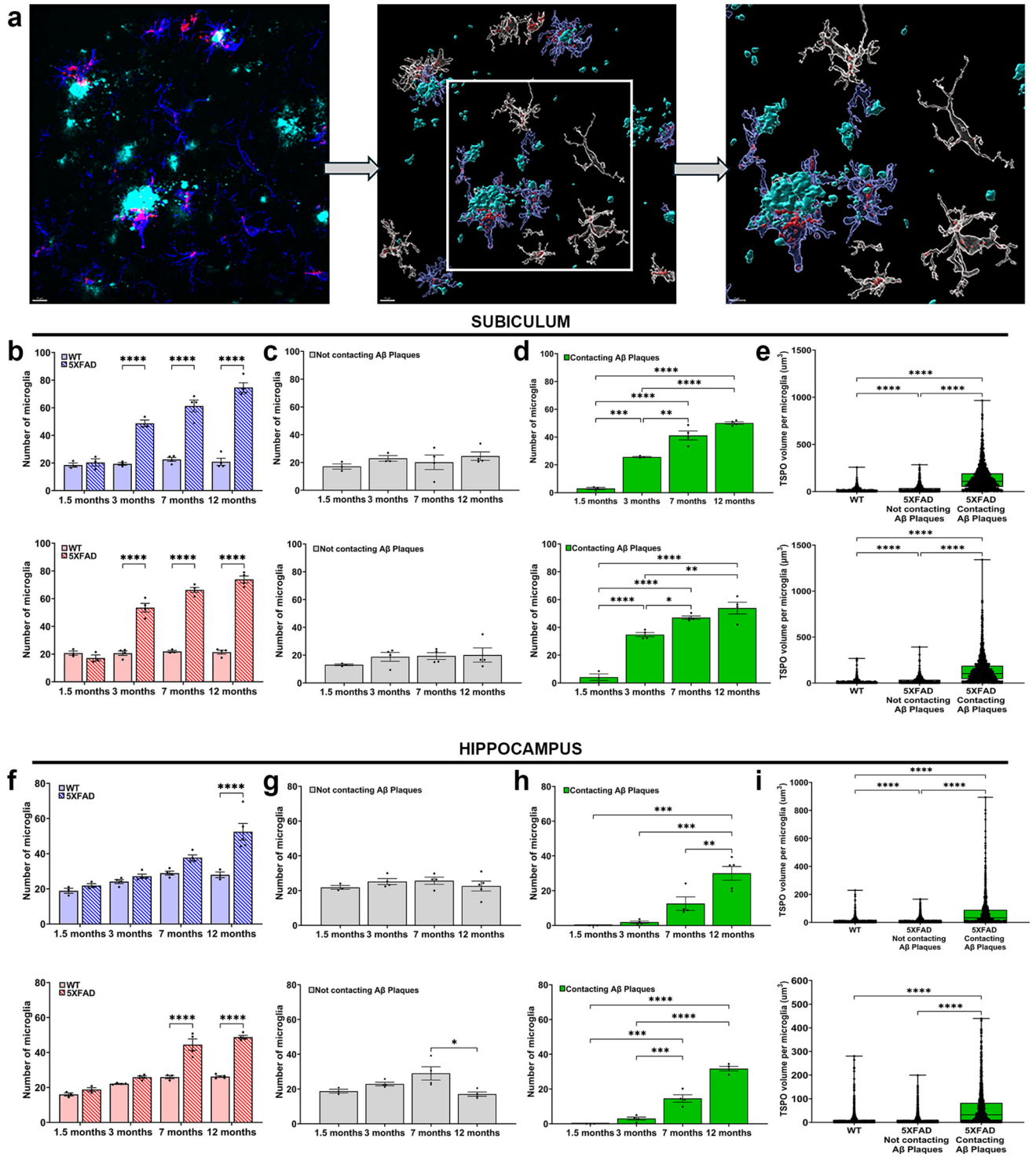

astrocytes since it is also expressed in synaptic terminals of glutamatergic neurons [64]. Similar to our present results in the 5XFAD mouse brain and in human LOAD cases, other human studies have shown no increase in astrocytic TSPO in the AD brain [37, 52]. Collectively, our findings have shown that the increase in TSPO levels with the progression of AD pathology in the 5XFAD mouse brain reflects activated microglia in close contact or embedded within Aβ-plaques, and these microglia expressed higher levels of TSPO relative to microglia not contacting plaques (Fig. 6).

We also examined postmortem brain tissue from *PSEN1-E280A* mutation AD cases, we found that TSPO levels were increased relative to controls using [^{3}H]-R-PK11195 quantitative autoradiography (Fig. 7a). Furthermore, like what

◂**Fig. 6** Analysis of microglia number, classification of microglia relevant to contacting Aβ plaques and TSPO volume per microglia in WT and 5XFAD mice. **a** Rendering process using a representative quadruple-label immunofluorescence confocal z-stack at 60X magnification. In the left panel is the immunofluorescence confocal image of Aβ (cyan), TSPO (red), and microglia (Iba-1; blue) in the subiculum of a 1.5 months 5XFAD female. The middle panel is the rendered image from Imaris showing Aβ (cyan), TSPO (red), microglia not contacting Aβ plaques (white) and microglia contacting Aβ plaques (blue), with the white square indicating the zoomed image presented in the right panel. Analysis of the number of microglia in the **b** subiculum and **f** hippocampus; the number of microglia not contacting Aβ plaques in the **c** subiculum and the **g** hippocampus; the number of microglia contacting Aβ plaques in the **d** subiculum and the **h** hippocampus; and TSPO volume per microglia (μm^3) (all the ages combined) in the **e** subiculum and **i** hippocampus-CA4 of male (top panels) and female (bottom panels) WT ($n = 3$–5) and 5XFAD ($n = 3$–5) mice. The number of microglia data were analyzed by two-way ANOVA (genotype and age) or one-way ANOVA (age) with Šídák's multiple comparisons test for comparisons by age-matched genotype. TSPO volume per microglia (μm^3) data were analyzed by the Kruskal–Wallis test with multiple comparisons Dunn's test by microglia proximity to Aβ plaques (not contacting and contacting) and genotype. All data are represented as mean ± SEM. $^{*}p < 0.05$, $^{**}p < 0.01$, $^{***}p < 0.001$, $^{****}p < 0.0001$. The volume of analysis for all images was 2.4696×10^7 μm^3. Complete statistical analysis for microglia number and TSPO volume results is presented in Suppl. Tables 16a, b and 20

we observed in the 5XFAD brain, the TSPO increase in the *PSEN1-E280A* mutation AD cases was due to an increased number of microglia (Fig. 7d) and an increase in TSPO levels per microglia, specifically in microglia that were in contact or embedded within Aβ-plaques (Fig. 7f and Suppl. Figure 7). The quantification of TSPO levels in microglia based on their classification of contacting or not contacting plaques in both the 5XFAD mouse brain and in *E280A* mutation carriers is a novel finding that has not been described previously and provides important insights for the interpretation of TSPO-PET imaging studies in AD.

Our current findings are consistent with a previous study analyzing the transcriptional signature of microglia associated with Aβ-plaques in AD patients in which they found that in $XO4^+$ microglia (microglia that phagocytize amyloid fragments), *TSPO* was one of the most highly upregulated genes in AD patients [30]. Another study using spatial transcriptomics to examine distinct microglia states in AD patients which were treated with Aβ immunization compared to non-immunized AD subjects, found that in cortical Aβ clusters enriched in microglia, *TSPO* was the second most upregulated gene [55]. Other studies have shown that TSPO-positive microglia clustering within, or surrounding Aβ-plaques have a $CD68^+$ phagocytic phenotype [27]. Another study [20] has also shown that these plaque-associated microglia could be carriers of Aβ fibrils to unaffected brain tissue. The latter is relevant to the present study because these are the same microglia that have a high TSPO content and targeting them with high affinity TSPO ligands may mitigate or reduced neuroinflammation and propagation of Aβ to unaffected brain regions. Combined, these previous studies and our present findings indicate that in AD, Aβ-plaque-associated microglia with a phagocytic phenotype may propagate AD pathology and these same microglia are the primary drivers of the TSPO increase in AD.

Our current findings are in contrast with a recent report by Nutma and colleagues indicating that the level of TSPO, the number of microglia, and the TSPO level per microglia did not change in postmortem human brain tissue from LOAD cases relative to brain tissue from healthy controls, although they did find a TSPO increase in mouse models of AD relative to WT [53]. They attributed this differential human versus rodent brain TSPO response to an evolutionary defined genetic divergence in the TSPO gene promoter. They noted that the increase in TSPO expression in activated myeloid cells depends on the transcription factor AP1 and was unique to a subset of rodent species but not in humans. However, this assertion is in contrast with several human TSPO-PET studies indicating that TSPO levels do increase in the brain of LOAD cases relative to age-matched controls [12, 28, 35, 80–82] as well as in animal models of AD [6, 8, 11, 25, 39, 50, 52, 70, 74, 77].

One potential explanation for this discrepancy in the rodent versus human TSPO response in the Nutma et al. study [53] may be that the human brain tissue was from LOAD cases classified as Braak stage 5–6 with an average age of 73 years of age and a standard deviation of 10 years, although individual ages were not provided. It is possible that at these older ages microglia may be dysfunctional and not able to upregulate TSPO when compared to the relatively younger brains from EOAD cases in our current study with an average age of AD cases of 58.3 years and a standard error of 4.4 years [19, 72]. This observation is consistent with a TSPO-PET study in AD subjects which found that EOAD patients had higher levels of TSPO binding than LOAD cases, [43] and TSPO levels increased with disease progression in EOAD cases but not in LOAD cases [42].

This explanation is also consistent with TSPO-PET imaging studies in which they find significant increases in TSPO levels in subjects with mild cognitive impairment (MCI) and in MCI cases that progress to AD [4]. In our study, we used postmortem brain tissue from EOAD cases classified with Braak stage 6 with an average age of disease onset of 49.2 ± 5.2 years and an average age at death of 58.3 ± 4.4 years which was similar in Braak stage but significantly differs in age from the Nutma et al. study [53]. Furthermore, in our study, the 5XFAD transgenic mouse findings were appropriately compared to early-onset *PSEN1-E280A* AD cases, since both have an aggressive AD phenotype in age of pathology and cognitive decline. This is important because new molecular approaches using single nuclei RNA sequencing and proteomics indicates distinct

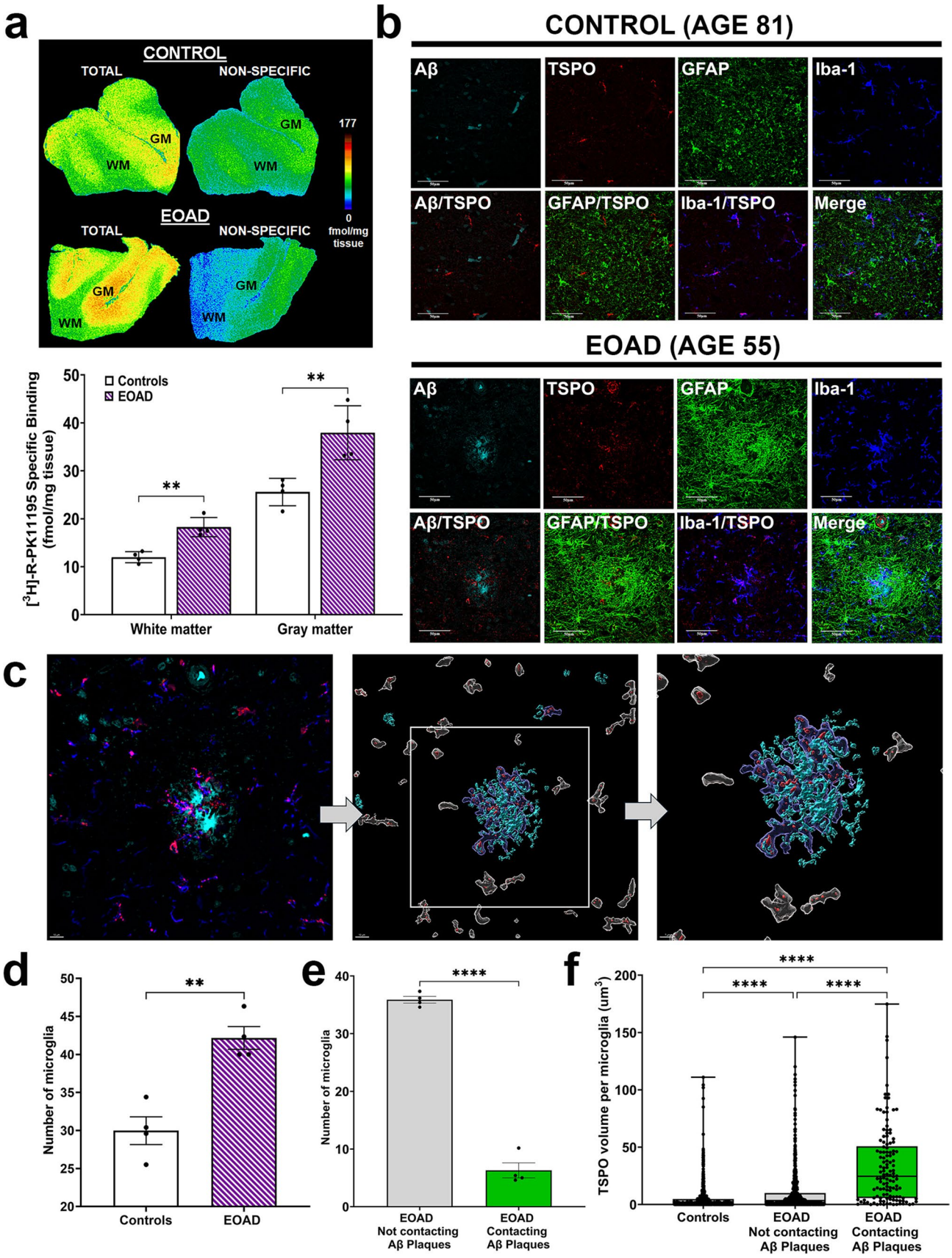
a
CONTROL
TOTAL
NON-SPECIFIC
GM
WM
177
0
fmol/mg tissue
EOAD
[3H]-R-PK11195 Specific Binding (fmol/mg tissue)
Controls
EOAD
White matter
Gray matter
b
CONTROL (AGE 81)
Aβ
TSPO
GFAP
Iba-1
Aβ/TSPO
GFAP/TSPO
Iba-1/TSPO
Merge
EOAD (AGE 55)
c
d
Number of microglia
Controls
EOAD
e
EOAD Not contacting Aβ Plaques
EOAD Contacting Aβ Plaques
f
TSPO volume per microglia (um3)

◂**Fig. 7** Analysis of brain TSPO levels, TSPO cellular sources, microglia number, and TSPO volume per microglia in controls and EOAD *PSEN1 E280A* mutation carriers. **a** (Top) Representative pseudocolor images with calibration bars showing total binding and non-specific binding of [^{3}H]-R-PK11195 autoradiography in the prefrontal cortex GM (gray matter) and WM (white matter) of controls and *PSEN1-E280A* mutation carriers (EOAD). (Bottom) Quantification of TSPO expression levels (fmol/mg tissue) in controls ($n=4$) and *PSEN1 E280A* mutation carriers (EOAD; $n=4$). **b** Representative quadruple-label immunofluorescence confocal imaging z-stacks of Aβ (cyan), TSPO (red), astrocytes (GFAP; green), and microglia (Iba-1; blue) in the temporal superior cortex of controls (top panels) and *PSEN1 E280A* mutation carriers (EOAD; bottom panels) at 60X magnification. **c** Representative rendering process using a quadruple-label immunofluorescence confocal z-stack at 60X magnification of Aβ (cyan), TSPO (red), and microglia (Iba-1; blue) in the temporal superior cortex from a *PSEN1 E280A* mutation carrier. The rendered image from Imaris shows Aβ (cyan), TSPO (red), microglia not contacting Aβ plaques (white) and microglia contacting Aβ plaques (blue), with the white square indicating the zoomed image presented in the right panel. Analysis of the **d** number of microglia, **e** number of microglia not contacting Aβ plaques and microglia contacting Aβ plaques, and **f** TSPO volume per microglia (μm^3) in the superior temporal cortex of controls ($n=4$) and *PSEN1-E280A* mutation carriers (EOAD; $n=4$). Data were analyzed by a two-sample t-test. TSPO volume per microglia data were analyzed by the Kruskal–Wallis Test with multiple comparisons Dunn's Test by microglia proximity to Aβ plaques (not contacting and contacting). All data are represented as mean ± SEM. $^{**}p<0.01$, $^{****}p<0.0001$. The volume of analysis for all images was 7.056×10^5 μm^3. Complete statistical analysis for studies with *PSEN1-E280A* mutation carriers is presented in Suppl. Tables 18a, b

and unique cellular mechanisms in EOAD and LOAD cases, which are defined by disease stage [3, 60].

Another possibility in the discrepancy between the Nutma et al. report [53] and our findings is that the images presented in their study did not include Aβ-plaque immunostaining in the same image with TSPO, microglia, and astrocyte immunostaining. Thus, it is possible that in their analysis, they could have selected microglia that were not in contact with Aβ-plaques, hence, explaining the lack of an increase in TSPO levels based on the observations in our present study. That is, microglia in contact with Aβ-plaques drive the increase in TSPO levels.

Our study has some limitations that need to be pointed out. First, we used a limited number of *PSEN1-E280A* AD cases and healthy controls, which calls for a larger study with a greater number of samples as well as the inclusion of LOAD brain tissue with age-matched controls. Lastly, all the human brain tissue samples in our study were from male subjects and the inclusion of female subjects is needed.

One of the biggest challenges in the diagnosis of AD and in the development of effective therapies is early patient identification [22]. Our findings in a preclinical AD model suggest the possibility of implementing TSPO as an early biomarker of neuroinflammation as a complement to other established AD biomarkers [36]. In addition, the discovery that TSPO levels first increased in the subiculum with the early aggregation of Amyloid-β suggests that the subiculum should be an area of focus in future TSPO-PET imaging studies in AD. Other studies have shown that the subiculum expresses the earliest atrophy in AD patients which predicted performance in memory scores [13]. Finally, it would be important from a therapeutic perspective to not only target clearance of Aβ-plaques from the brain, but also combine it with high affinity TSPO ligands to target Aβ-plaque-associated microglia with high TSPO content to reduce neuroinflammation at the early stage of the disease and potentially inhibit the propagation of Aβ fibrils to unaffected brain regions.

Supplementary Information The online version contains supplementary material available at https://doi.org/10.1007/s00401-025-02912-4.

Acknowledgements While this manuscript was in preparation, we learned of the death of our great friend and colleague Dr. Francisco Lopera. Dr. Lopera was an outstanding neurologist and human being who discovered the PSEN1-E280A mutation (the Paisa mutation) in a most unique cohort of Alzheimer's disease patients in the region of Antioquia, Colombia. Not only did he care for his patients as a physician but also as a human being that dreamed of establishing a city named Villa Aliria where these unique cases could live and be served with a better life than their genes dictated. May he rest in peace and one day "see" an effective solution to this most devastating disease.

Author contributions Concept and design: T.R.G., D.A.M.P., J.L.M. Tissue acquisition and processing: D.A.M.P., J.L.M., A.N.R., F.L., C.A.V.L. Neuropathology: D.A.M.P., C.A.V.L. Experimental methods: T.R.G., D.A.M.P., J.L.M., A.N.R., K.A. Analysis and interpretation of the data: T.R.G., D.A.M.P., J.L.M., Z.B. Drafting of the manuscript: T.R.G., D.A.M.P., J.L.M. Critical revision of the manuscript: all the authors.

Funding This work was supported by grants ES007062-24 to T.R.G. from the National Institute of Environmental Health Sciences (NIEHS), ES007062-23S1 to T.R.G. from the National Institute on Aging, and T32-ES033955 to A.N.R. from the NIEHS.

Data availability All raw data are available by request to the corresponding author.

Declarations

Conflict of interest The authors declare no competing interests.

References

1. Acosta-Baena N, Sepulveda-Falla D, Lopera-Gómez CM, Jaramillo-Elorza MC, Moreno S, Aguirre-Acevedo DC et al (2011) Pre-dementia clinical stages in presenilin 1 E280A familial early-onset Alzheimer's disease: a retrospective cohort study. Lancet Neurol 10:213–220. https://doi.org/10.1016/S1474-4422(10)70323-9
2. Aguirre-Acevedo DC, Lopera F, Henao E, Tirado V, Muñoz C, Giraldo M et al (2016) Cognitive decline in a colombian kindred with autosomal dominant Alzheimer disease a retrospective cohort study. JAMA Neurol 73:431–438. https://doi.org/10.1001/jamaneurol.2015.4851
3. Almeida MC, Eger SJ, He C, Audouard M, Nikitina A, Glasauer SMK et al (2024) Single-nucleus RNA sequencing demonstrates an autosomal dominant Alzheimer's disease profile and possible mechanisms of disease protection. Neuron 112:1778-1794.e7. https://doi.org/10.1016/j.neuron.2024.02.009
4. Appleton J, Finn Q, Zanotti-Fregonara P, Yu M, Faridar A, Nakawah MO et al (2024) Brain inflammation co-localizes highly with tau in mild 2 cognitive impairment due to early-onset Alzheimer's disease. Brain
5. Attar A, Liu T, Chan WTC, Hayes J, Nejad M, Lei KC et al (2013) A shortened barnes maze protocol reveals memory deficits at 4-months of age in the triple-transgenic mouse model of Alzheimer's disease. PLoS ONE. https://doi.org/10.1371/journal.pone.0080355
6. Barron AM, Tokunaga M, Zhang MR, Ji B, Suhara T, Higuchi M (2016) Assessment of neuroinflammation in a mouse model of obesity and β-amyloidosis using PET. J Neuroinflammation 13:1–14. https://doi.org/10.1186/s12974-016-0700-x
7. Betlazar C, Harrison-Brown M, Middleton RJ, Banati R, Liu GJ (2018) Cellular sources and regional variations in the expression of the neuroinflammatory marker translocator protein (TSPO) in the normal brain. Int J Mol Sci. https://doi.org/10.3390/ijms19092707
8. Biechele G, Franzmeier N, Blume T, Ewers M, Luque JM, Eckenweber F et al (2020) Glial activation is moderated by sex in response to amyloidosis but not to tau pathology in mouse models of neurodegenerative diseases. J Neuroinflammation 17:1–10. https://doi.org/10.1186/s12974-020-02046-2
9. Botella Lucena P, Vanherle S, Lodder C, Gutiérrez de Ravé M, Stancu IC, Lambrichts I et al (2022) Blood-based Aβ42 increases in the earliest pre-pathological stage before decreasing with progressive amyloid pathology in preclinical models and human subjects: opening new avenues for prevention. Acta Neuropathol 144:489–508. https://doi.org/10.1007/s00401-022-02458-9
10. Bradburn S, Murgatroyd C, Ray N (2019) Neuroinflammation in mild cognitive impairment and Alzheimer's disease: a meta-analysis. Ageing Res Rev 50:1–8. https://doi.org/10.1016/j.arr.2019.01.002
11. Brendel M, Probst F, Jaworska A, Overhoff F, Korzhova V, Albert NL et al (2016) Glial activation and glucose metabolism in a transgenic amyloid mouse model: a triple-tracer PET study. J Nucl Med 57:954–960. https://doi.org/10.2967/jnumed.115.167858
12. Canário N, Jorge L, Martins R, Santana I, Castelo-Branco M (2022) Dual PET-fMRI reveals a link between neuroinflammation, amyloid binding and compensatory task-related brain activity in Alzheimer's disease. Commun Biol 5:1–7. https://doi.org/10.1038/s42003-022-03761-7
13. Carlesimo GA, Piras F, Orfei MD, Iorio M, Caltagirone C, Spalletta G (2015) Atrophy of presubiculum and subiculum is the earliest hippocampal anatomical marker of Alzheimer's disease. Alzheimer's Dement Diagnosis, Assess Dis Monit 1:24–32. https://doi.org/10.1016/j.dadm.2014.12.001
14. Chaney A, Bauer M, Bochicchio D, Smigova A, Kassiou M, Davies KE et al (2018) Longitudinal investigation of neuroinflammation and metabolite profiles in the APP swe ×PS1 Δe9 transgenic mouse model of Alzheimer's disease. J Neurochem 144:318–335. https://doi.org/10.1111/jnc.14251
15. Chatterjee P, Pedrini S, Doecke JD, Thota R, Villemagne VL, Doré V et al (2023) Plasma Aβ42/40 ratio, *p*-tau181, GFAP, and NfL across the Alzheimer's disease continuum: a cross-sectional and longitudinal study in the AIBL cohort. Alzheimer's Dement 19:1117–1134. https://doi.org/10.1002/alz.12724
16. Chauveau F, Boutin H, Van Camp N, Dollé F, Tavitian B (2008) Nuclear imaging of neuroinflammation: a comprehensive review of [11C]PK11195 challengers. Eur J Nucl Med Mol Imaging 35:2304–2319. https://doi.org/10.1007/s00259-008-0908-9
17. Chen MK, Guilarte TR (2008) Translocator protein 18 kDa (TSPO): Molecular sensor of brain injury and repair. Pharmacol Ther 118:1–17. https://doi.org/10.1016/j.pharmthera.2007.12.004
18. Clayton K, Delpech JC, Herron S, Iwahara N, Ericsson M, Saito T et al (2021) Correction to: Plaque associated microglia hyper-secrete extracellular vesicles and accelerate tau propagation in a humanized APP mouse model (Molecular Neurodegeneration, (2021), 16, 1, (18), DOI: 10.1186/s13024-021-00440-9). Mol Neurodegener 16:1–16. https://doi.org/10.1186/s13024-021-00447-2
19. Costa J, Martins S, Ferreira PA, Cardoso AMS, Guedes JR, Peça J et al (2021) The old guard: age-related changes in microglia and their consequences. Mech Ageing Dev. https://doi.org/10.1016/j.mad.2021.111512
20. d'Errico P, Ziegler-Waldkirch S, Aires V, Hoffmann P, Mezö C, Erny D et al (2022) Microglia contribute to the propagation of Aβ into unaffected brain tissue. Nat Neurosci 25:20–25. https://doi.org/10.1038/s41593-021-00951-0
21. Doecke JD, Pérez-Grijalba V, Fandos N, Fowler C, Villemagne VL, Masters CL et al (2020) Total Aβ42/Aβ40 ratio in plasma predicts amyloid-PET status, independent of clinical AD diagnosis. Neurology 94:E1580–E1591. https://doi.org/10.1212/WNL.0000000000009240
22. Dokholyan NV, Mohs RC, Bateman RJ (2022) Challenges and progress in research, diagnostics, and therapeutics in Alzheimer's disease and related dementias. Alzheimer's Dement Transl Res Clin Interv 8:1–5. https://doi.org/10.1002/trc2.12330
23. Fleisher AS, Chen K, Quiroz YT, Jakimovich LJ, Gomez MG, Langois CM et al (2012) Florbetapir PET analysis of amyloid-β deposition in the presenilin 1 E280A autosomal dominant Alzheimer's disease kindred: a cross-sectional study. Lancet Neurol 11:1057–1065. https://doi.org/10.1016/S1474-4422(12)70227-2
24. Floden AM, Combs CK (2011) Microglia demonstrate age-dependent interaction with amyloid-β fibrils. J Alzheimer's Dis 25:279–293. https://doi.org/10.3233/JAD-2011-101014
25. Focke C, Blume T, Zott B, Shi Y, Deussing M, Peters F et al (2019) Early and longitudinal microglial activation but not amyloid accumulation predicts cognitive outcome in PS2APp mice. J Nucl Med 60:548–554. https://doi.org/10.2967/jnumed.118.217703
26. Forner S, Kawauchi S, Balderrama-Gutierrez G, Kramár EA, Matheos DP, Phan J et al (2021) Systematic phenotyping and characterization of the 5xFAD mouse model of Alzheimer's disease. Sci Data 8:1–16. https://doi.org/10.1038/s41597-021-01054-y
27. Garland EF, Antony H, Kulagowska L, Scott T, Rogien C, Bottlaender M et al (2024) The microglial translocator protein (TSPO) in Alzheimer's disease reflects a phagocytic phenotype. Acta Neuropathol. https://doi.org/10.1007/s00401-024-02822-x
28. Garland EF, Dennett O, Lau LC, Chatelet DS, Bottlaender M, Nicoll JAR et al (2023) The mitochondrial protein TSPO in Alzheimer's disease: relation to the severity of AD pathology and the

neuroinflammatory environment. J Neuroinflammation 20:1–15. https://doi.org/10.1186/s12974-023-02869-9
29. Giudici KV, De Souto BP, Guyonnet S, Li Y, Bateman RJ, Vellas B (2020) Assessment of plasma amyloid-β42/40and cognitive decline among community-dwelling older adults. JAMA Netw Open 3:1–13. https://doi.org/10.1001/jamanetworkopen.2020.28634
30. Grubman A, Choo XY, Chew G, Ouyang JF, Sun G, Croft NP et al (2021) Transcriptional signature in microglia associated with Aβ plaque phagocytosis. Nat Commun. https://doi.org/10.1038/s41467-021-23111-1
31. Guilarte TR (2019) TSPO in diverse CNS pathologies and psychiatric disease: a critical review and a way forward. Pharmacol Ther 194:44–58. https://doi.org/10.1016/j.physbeh.2017.03.040
32. Guilarte TR, Rodichkin AN, McGlothan JL, Acanda De La Rocha AM, Azzam DJ (2021) Imaging neuroinflammation with TSPO: A new perspective on the cellular sources and subcellular localization. Pharmacol Ther. https://doi.org/10.1016/j.pharmthera.2021.108048
33. Hamelin L, Lagarde J, Dorothée G, Leroy C, Labit M, Comley RA et al (2016) Early and protective microglial activation in Alzheimer's disease: a prospective study using 18F-DPA-714 PET imaging. Brain 139:1252–1264. https://doi.org/10.1093/brain/aww017
34. Hamelin L, Lagarde J, Dorothée G, Potier MC, Corlier F, Kuhnast B et al (2018) Distinct dynamic profiles of microglial activation are associated with progression of Alzheimer's disease. Brain 141:1855–1870. https://doi.org/10.1093/brain/awy079
35. Hommet C, Mondon K, Camus V, Ribeiro MJ, Beaufils E, Arlicot N et al (2014) Neuroinflammation and β amyloid deposition in alzheimer's disease: In vivo quantification with molecular imaging. Dement Geriatr Cogn Disord 37:1–18. https://doi.org/10.1159/000354363
36. Jack CR, Andrews JS, Beach TG, Buracchio T, Dunn B, Graf A et al (2024) Revised criteria for diagnosis and staging of Alzheimer's disease: Alzheimer's Association Workgroup. Alzheimer's Dement 20:5143–5169. https://doi.org/10.1002/alz.13859
37. Ji B, Ono M, Yamasaki T, Fujinaga M, Zhang MR, Seki C et al (2021) Detection of Alzheimer's disease-related neuroinflammation by a PET ligand selective for glial versus vascular translocator protein. J Cereb Blood Flow Metab 41:2076–2089. https://doi.org/10.1177/0271678X21992457
38. Kang S, Kim J, Lee SY, Okamura N, Chang KA (2022) MicroPET imaging assessment of brain tau and amyloid deposition in 6 × Tg Alzheimer's disease model mice. Int J Mol Sci. https://doi.org/10.3390/ijms23105485
39. Keller T, López-Picón FR, Krzyczmonik A, Forsback S, Kirjavainen AK, Takkinen JS et al (2018) [18 F]F-DPA for the detection of activated microglia in a mouse model of Alzheimer's disease. Nucl Med Biol 67:1–9. https://doi.org/10.1016/j.nucmedbio.2018.09.001
40. Komada M, Takao K, Miyakawa T (2008) Elevated plus maze for mice. J Vis Exp. https://doi.org/10.3791/1088
41. Krabbe G, Halle A, Matyash V, Rinnenthal JL, Eom GD, Bernhardt U et al (2013) Functional impairment of microglia coincides with beta-amyloid deposition in mice with alzheimer-like pathology. PLoS ONE. https://doi.org/10.1371/journal.pone.0060921
42. Kreisl WC, Lyoo CH, Liow JS, Wei M, Snow J, Page E et al (2016) 11C-PBR28 binding to translocator protein increases with progression of Alzheimer's disease. Neurobiol Aging 44:53–61. https://doi.org/10.1016/j.neurobiolaging.2016.04.011
43. Kreisl WC, Lyoo CH, McGwier M, Snow J, Jenko KJ, Kimura N et al (2013) In vivo radioligand binding to translocator protein correlates with severity of Alzheimer's disease. Brain 136:2228–2238. https://doi.org/10.1093/brain/awt145
44. Kumar A, Muzik O, Shandal V, Chugani D, Chakraborty P, Chugani HT (2012) Evaluation of age-related changes in translocator protein (TSPO) in human brain using 11C-[R]-PK11195 PET. J Neuroinflammation. https://doi.org/10.1186/1742-2094-9-232
45. Kwon HS, Koh SH (2020) Neuroinflammation in neurodegenerative disorders: the roles of microglia and astrocytes. Transl Neurodegener 9:1–12. https://doi.org/10.1186/s40035-020-00221-2
46. Landel V, Baranger K, Virard I, Loriod B, Khrestchatisky M, Rivera S et al (2014) Temporal gene profiling of the 5XFAD transgenic mouse model highlights the importance of microglial activation in Alzheimer's disease. Mol Neurodegener 9:1–18. https://doi.org/10.1186/1750-1326-9-33
47. Leng F, Edison P (2021) Neuroinflammation and microglial activation in Alzheimer disease: Where do we go from here? Nat Rev Neurol 17:157–172. https://doi.org/10.1038/s41582-020-00435-y
48. Liu B, Le KX, Park MA, Wang S, Belanger AP, Dubey S et al (2015) In vivo detection of age-and disease-related increases in neuroinflammation by18F-GE180 TSPO microPET imaging in wild-type and alzheimer's transgenic mice. J Neurosci 35:15716–15730. https://doi.org/10.1523/JNEUROSCI.0996-15.2015
49. Long JM, Holtzman DM (2019) Alzheimer disease: an update on pathobiology and treatment strategies. Cell 179:312–339. https://doi.org/10.1016/j.cell.2019.09.001
50. López-Picón FR, Snellman A, Eskola O, Helin S, Solin O, Haaparanta-Solin M et al (2018) Neuroinflammation appears early on PET imaging and then plateaus in a mouse model of Alzheimer disease. J Nucl Med 59:509–515. https://doi.org/10.2967/jnumed.117.197608
51. Loth MK, Choi J, McGlothan JL, Pletnikov MV, Pomper MG, Guilarte TR (2016) TSPO in a murine model of Sandhoff disease: presymptomatic marker of neurodegeneration and disease pathophysiology. Neurobiol Dis 85:174–186. https://doi.org/10.1016/j.nbd.2015.11.001
52. Mirzaei N, Tang SP, Ashworth S, Coello C, Plisson C, Passchier J et al (2016) In vivo imaging of microglial activation by positron emission tomography with [11C]PBR28 in the 5XFAD model of Alzheimer's disease. Glia 64:993–1006. https://doi.org/10.1002/glia.22978
53. Nutma E, Fancy N, Weinert M, Tsartsalis S, Marzin MC, Muirhead RCJ et al (2023) Translocator protein is a marker of activated microglia in rodent models but not human neurodegenerative diseases. Nat Commun. https://doi.org/10.1038/s41467-023-40937-z
54. Oakley H, Cole SL, Logan S, Maus E, Shao P, Craft J et al (2006) Intraneuronal β-amyloid aggregates, neurodegeneration, and neuron loss in transgenic mice with five familial Alzheimer's disease mutations: Potential factors in amyloid plaque formation. J Neurosci 26:10129–10140. https://doi.org/10.1523/JNEUROSCI.1202-06.2006
55. van Olst L, Simonton B, Edwards AJ, Forsyth AV, Boles J, Jamshidi P et al (2025) Microglial mechanisms drive amyloid-β clearance in immunized patients with Alzheimer's disease. Nat Med. https://doi.org/10.1038/s41591-025-03574-1
56. Owen DR, Yeo AJ, Gunn RN, Song K, Wadsworth G, Lewis A et al (2012) An 18-kDa Translocator Protein (TSPO) polymorphism explains differences in binding affinity of the PET radioligand PBR28. J Cereb Blood Flow Metab 32:1–5. https://doi.org/10.1038/jcbfm.2011.147
57. Owen DRJ, Gunn RN, Rabiner EA, Bennacef I, Fujita M, Kreisl WC et al (2011) Mixed-affinity binding in humans with 18-kDa translocator protein ligands. J Nucl Med 52:24–32. https://doi.org/10.2967/jnumed.110.079459
58. Papadopoulos V, Baraldi M, Guilarte TR, Knudsen TB, Lacapère JJ, Lindemann P et al (2006) Translocator protein (18 kDa): new nomenclature for the peripheral-type benzodiazepine receptor based on its structure and molecular function. Trends Pharmacol Sci 27:402–409. https://doi.org/10.1016/j.tips.2006.06.005

59. Pascoal TA, Benedet AL, Ashton NJ, Kang MS, Therriault J, Chamoun M et al (2021) Microglial activation and tau propagate jointly across Braak stages. Alzheimer's Dement 17:1–2. https://doi.org/10.1002/alz.056653
60. Pichet Binette A, Gaiteri C, Wennström M, Kumar A, Hristovska I, Spotorno N et al (2024) Proteomic changes in Alzheimer disease associated with progressive Aβ plaque and tau tangle pathologies. Nat Neurosci. https://doi.org/10.1038/s41593-024-01737-w
61. Pitts M (2018) Barnes maze procedure for spatial learning and memory in mice. Bio-Protoc 8:1–11. https://doi.org/10.21769/bioprotoc.2744
62. Rauchmann BS, Brendel M, Franzmeier N, Trappmann L, Zaganjori M, Ersoezlue E et al (2022) Microglial activation and connectivity in Alzheimer disease and aging. Ann Neurol 92:768–781. https://doi.org/10.1002/ana.26465
63. Rejc L, Gómez-Vallejo V, Joya A, Arsequell G, Egimendia A, Castellnou P et al (2022) Longitudinal evaluation of neuroinflammation and oxidative stress in a mouse model of Alzheimer disease using positron emission tomography. Alzheimer's Res Ther 14:1–14. https://doi.org/10.1186/s13195-022-01016-5
64. Rimmele TS, Rosenberg PA (2016) GLT-1: The elusive presynaptic glutamate transporter. Neurochem Int 98:19–28. https://doi.org/10.1016/j.neuint.2016.04.010
65. Rodichkin AN, Edler MK, McGlothan JL, Guilarte TR (2021) Behavioral and neurochemical studies of inherited manganese-induced dystonia-parkinsonism in Slc39a14-knockout mice. Neurobiol Dis. https://doi.org/10.1016/j.nbd.2021.105467
66. Rojas C, Stathis M, Coughlin JM, Pomper M, Slusher BS (2018) The low-affinity binding of second generation radiotracers targeting TSPO is associated with a unique allosteric binding site. J Neuroimmune Pharmacol 13:1–5. https://doi.org/10.1007/s11481-017-9765-2
67. Rossano SM, Johnson AS, Smith A, Ziaggi G, Roetman A, Guzman D et al (2024) Microglia measured by TSPO PET are associated with Alzheimer's disease pathology and mediate key steps in a disease progression model. Alzheimer's Dement. https://doi.org/10.1002/alz.13699
68. Sahrai H, Norouzi A, Hamzehzadeh S, Majdi A, Kahfi-Ghaneh R, Sadigh-Eteghad S (2023) SIMOA-based analysis of plasma NFL levels in MCI and AD patients: a systematic review and meta-analysis. BMC Neurol 23:1–12. https://doi.org/10.1186/s12883-023-03377-2
69. Selkoe DJ, Hardy J (2016) The amyloid hypothesis of Alzheimer's disease at 25 years. EMBO Mol Med 8:595–608. https://doi.org/10.15252/emmm.201606210
70. Sérrière S, Tauber C, Vercouillie J, Mothes C, Pruckner C, Guilloteau D et al (2015) Amyloid load and translocator protein 18kDa in APPswePS1-dE9 mice: a longitudinal study. Neurobiol Aging 36:1639–1652. https://doi.org/10.1016/j.neurobiolaging.2014.11.023
71. Thal DR, Rüb U, Orantes M, Braak H (2002) Phases of Aß-deposition in the human brain and its relevance for the development of AD. Neurology 58:1791–1800. https://doi.org/10.1212/WNL.58.12.1791
72. Thomas AL, Lehn MA, Janssen EM, Hildeman DA, Chougnet CA (2022) Naturally-aged microglia exhibit phagocytic dysfunction accompanied by gene expression changes reflective of underlying neurologic disease. Sci Rep 12:1–10. https://doi.org/10.1038/s41598-022-21920-y
73. Toppala S, Ekblad LL, Tuisku J, Helin S, Johansson JJ, Laine H et al (2021) Association of early β-amyloid accumulation and neuroinflammation measured With [11C]PBR28 in elderly individuals without dementia. Neurology 96:E1608–E1619. https://doi.org/10.1212/WNL.0000000000011612
74. Tournier BB, Tsartsalis S, Ceyzériat K, Fraser BH, Grégoire MC, Kövari E et al (2020) Astrocytic TSPO upregulation appears before microglial TSPO in Alzheimer's disease. J Alzheimer's Dis 77:1043–1056. https://doi.org/10.3233/JAD-200136
75. Tournier BB, Tsartsalis S, Ceyzériat K, Medina Z, Fraser BH, Grégoire MC et al (2020) Fluorescence-activated cell sorting to reveal the cell origin of radioligand binding. J Cereb Blood Flow Metab 40:1242–1255. https://doi.org/10.1177/0271678X19860408
76. Tournier BB, Tsartsalis S, Rigaud D, Fossey C, Cailly T, Fabis F et al (2019) TSPO and amyloid deposits in sub-regions of the hippocampus in the 3xTgAD mouse model of Alzheimer's disease. Neurobiol Dis 121:95–105. https://doi.org/10.1016/j.nbd.2018.09.022
77. Tsukada H, Nishiyama S, Ohba H, Kanazawa M, Kakiuchi T, Harada N (2014) Comparing amyloid-β deposition, neuroinflammation, glucose metabolism, and mitochondrial complex I activity in brain: a PET study in aged monkeys. Eur J Nucl Med Mol Imaging 41:2127–2136. https://doi.org/10.1007/s00259-014-2821-8
78. Tuisku J, Plavén-Sigray P, Gaiser EC, Airas L, Al-Abdulrasul H, Brück A et al (2019) Effects of age, BMI and sex on the glial cell marker TSPO—a multicentre [11C]PBR28 HRRT PET study. Eur J Nucl Med Mol Imaging 46:2329–2338. https://doi.org/10.1007/s00259-019-04403-7
79. Walf AA, Frye CA (2007) The use of the elevated plus maze as an assay of anxiety-related behavior in rodents. Nat Protoc 2:322–328. https://doi.org/10.1038/nprot.2007.44
80. Wang Q, Chen G, Schindler SE, Christensen J, McKay NS, Liu J et al (2022) Baseline microglial activation correlates with brain amyloidosis and longitudinal cognitive decline in Alzheimer disease. Neurol Neuroimmunol NeuroInflammation 9:1–11. https://doi.org/10.1212/NXI.0000000000001152
81. Yang Z, Banks SJ, Ritter AR, Cummings JL, Sreenivasan K, Kinney JW et al (2023) Microglial imaging in Alzheimer's disease and its relationship to brain amyloid: a human 18F-GE180 PET study. J Alzheimer's Dis 96:1505–1514. https://doi.org/10.3233/JAD-230631
82. Zhou R, Ji B, Kong Y, Qin L, Ren W, Guan Y et al (2021) PET imaging of neuroinflammation in Alzheimer's disease. Front Immunol 12:1–16. https://doi.org/10.3389/fimmu.2021.739130